Modelling of the flow of stable air over a complex region

Initial theoretical analysis of Richards Bay data

M T Scholtz and C J Brouckaert

A report of the Committee for Lower Atmosphere
National Programme for Environmental Sciences

SOUTH AFRICAN NATIONAL SCIENTIFIC PROGRAMMES REPORT NO

9

Issued by the
National Scientific Programmes Unit
Council for Scientific and Industrial Research
P O Box 395
PRETORIA 0001
from whom copies of reports in this series are available on request.

Printed 1976 in the Republic of South Africa
by S. Durrant & Viljoen (Pty) Ltd.

ISBN 0 7988 0943 4

Authors' addresses -

Dr M T Scholtz
Department of Chemical Engineering
University of Natal
King George V Avenue
DURBAN 4001

C J Brouckaert
c/o Department of Chemical Engineering
University of Natal
King George V Avenue
DURBAN 4001

PREFACE

The National Programme for Environmental Sciences is one of several national scientific programmes administered by the CSIR. It aims at identifying environmental problems in South Africa which lend themselves to solution through cooperative research and at promoting and coordinating research which will contribute to the solution of such problems. The National Programme includes research relating to environmental problems in the lower atmosphere, inland waters, the sea and terrestrial ecosystems. It is designed to meet both national and international objectives and it contributes to the international programme of SCOPE (Scientific Committee on Problems of the Environment), the body set up in 1970 by ICSU (International Council for Scientific Unions) to act as a focus of non-governmental international scientific effort in the environmental field. The Lower Atmosphere Section of the National Programme is concerned chiefly with mesometeorological research relating to the dispersion and transport of pollutants in the atmosphere, mesoclimatic changes in urban areas and research and surveillance relating to air pollution and possible climatic change in southern Africa.

The field work programme described in this report was carried out in the Richards Bay area, an area on the Natal coast approximately 190 km by road north of Durban. The funding received from the National Committee for Environmental Sciences for this work is gratefully acknowledged. The authors are also grateful to the Atomic Energy Board for their assistance with the design and construction of the data telemetry system, to the AE&CI Pollution Research Group at the University of Natal for financial assistance and loan of equipment, to the Richards Bay Town Board for their cooperation, and to the Council for Scientific and Industrial Research for funding in the form of a post-graduate bursary. Others who played major roles in the field work program were Mr M Mulholland (post-graduate student), Mr D Penn (Chief Technician) and Mr B Sharp (Research Technician).

SINOPSIS

Die vloei van stabiele lug oor 'n algemene landstreek van ingewikkelde topografie en nie-uniforme oppervlakte-temperatuur is ondersoek. Om 'n beter begrip van die beweging van oppervlakte-lug te verkry, was dit nodig om die vertikale windstruktuur vir stabiele lug wat teen 'n helling beweeg te bestudeer. 'n Teoretiese model word voorgestel om die vertikale struktuur te beskryf. Die model toon redelike ooreenstemming met eksperimentele data wat by Richardsbaai ingewin is. Die gevolgtrekkings word gemaak dat die Corioliskrag en die tempo van afwaartse momentumoordrag van die boliggende geostrofiese wind verontagsaam kan word in die oppervlakte-luglaag en dat die lugbeweging primêr bepaal word deur die verspreiding van oppervlaktedruk en die topografie. 'n Oppervlakte-windveldmodel gebaseer op bostaande bevindings en die kontinuïteitsvergelyking word voorgestel. Die data benodig vir die modelberekenings is die topografiese koördinate, land- en seetemperatuur, temperatuurinversie-sterkte en die heersende sinoptiese drukgradiënt. Die model sluit twee konstantes in wat empiries bepaal is. Daar is gevind dat die berekende windvelde goeie ooreenstemming toon met die windvelddata ingewin by Richardsbaai.

SYNOPSIS

The flow of stable air over a general region of complex topography and non-uniform surface temperature has been investigated. In order to gain further understanding of the motion of surface air, it was necessary to study the vertical structure of the wind for stable air moving on a slope. A theoretical model is proposed to describe the vertical structure and this was found to be in reasonable agreement with experimental data taken at Richards Bay. From this study it was concluded that the Coriolis force and rate of downward momentum transfer from the overlying geostrophic wind could be neglected in the surface air layer, and air motion is determined primarily by the distribution of surface pressure and the topographical relief. A surface wind field model is proposed, based on the above findings and the continuity equation. Inputs for model computations are topographic coordinates, land and sea temperatures, temperature inversion strength and the prevailing synoptic pressure gradient. The model includes two constants, which were empirically determined. The computed wind fields were found to be in good agreement with wind field data taken at Richards Bay.

CURRENT TITLES IN THIS SERIES

1. A description of the Savanna Ecosystem Project, Nylsvley, South Africa. December 1975. 24 pp.

2. Sensitivity analysis of a simple linear model of a savanna ecosystem at Nylsvley. W M Getz and A M Starfield. December 1975. 18 pp.

3. Savanna Ecosystem Project - Progress report 1974/1975. S M Hirst. December 1975. 27 pp.

4. Solid wastes research in South Africa. R G Noble. June 1976. 13 pp.

5. Bibliography on marine pollution in South Africa. D A Darracott and C E Cloete. June 1976. 131 pp.

6. Recycling and disposal of plastics waste in South Africa. R H Nurse, N C Symington, G R de V Brooks and L J Heyl. June 1976. 35 pp.

7. South African Red Data Book - Aves. W R Siegfried, P G H Frost, J Cooper and A C Kemp. June 1976. 108 pp.

8. South African marine pollution survey report 1974-1975. C E Cloete and W D Oliff (editors). September 1976. 60 pp.

9. Modelling of the flow of stable air over a complex region. M T Scholtz and C J Brouckaert. September 1976. 42 pp.

TABLE OF CONTENTS

LIST OF FIGURES

INTRODUCTION

One of the prime considerations in the development planning of new areas is the environmental impact of industries located in the area. The zoning for residential and industrial development should be such that amongst other considerations, the incidence of severe air pollution in urban areas is minimised. In order to carry out such rational planning it is necessary to make a comprehensive field study of both the micro- and meso-meteorology of the area. These site evaluation studies are expensive, take in most cases more than a year to complete and frequently the data which one can reasonably obtain from a field study do not provide sufficient information for the detailed planning of an area. The first objective of the research work discussed in this paper is the development of a general theoretical model which should predict the features of the micro- and meso-meteorology of a complex region and in particular the wind fields associated with stable conditions, so as to permit rapid site evaluations with a minimum of experimental effort. The second objective of the work is the modelling of stable wind fields for use with a dispersion model for dosage area prediction.

The incidence of severe atmospheric pollution is highest during periods when the lower atmosphere is stably stratified and wind speeds are low. Such conditions occur mainly during the night hours and persist into the mid-morning. The theoretical and experimental work has therefore been restricted to the flow of strongly stable air over a region of complex topography under these conditions.

Anderson (1971) has proposed a windfield model which is consistent with the continuity equation. This model indicates that the mesoscale perturbance of the ground level wind fields is mainly due to topography and ground temperature anomalies such as a land/sea interface or an urban heat island. The assumptions made in Anderson's work imply that his results are more applicable to a neutral or superadiabatic surface layer which is of greater thickness than the shallower, stable surface layer presently being considered. It has, however, been possible to modify some of the methods given by Anderson for the present work.

It is found in the present study that, in order to usefully describe the air movement over a region, theoretical models for predicting the wind fields of surface air movement as well as the vertical structure of wind speed and direction are necessary. Two such models are proposed and compared with experimental data taken in the Richards Bay area situated on the east coast of Natal, 160 km north of Durban.

In the Richards Bay area conditions of strong atmospheric stability are most frequent during the winter months (April through to mid-August) and are infrequent at other times of the year.

The work presently being reported is part of an overall program which has as its objective the modelling of dispersion and the prediction of dosage areas in a general region of complex topography. It should be noted that the work presently reported constitutes a theoretical basis for the analysis of data and the wind fields reported do not necessarily summarize the prevailing stable flows in the Richards Bay area.

The field work was carried out in the Richards Bay area during the period 1974-75 as part of the National Programme for Environmental Sciences, Lower Atmosphere Section.

THEORETICAL

In order to understand more fully the movement of stable air over a complex region, the vertical profiles of wind speed and direction for stable air moving over a slope have been investigated. This has led to further understanding of the motion of stable air close to the surface and has facilitated the modelling of the surface wind fields in a complex region.

Vertical structure model

The main features of the model are shown in Figure 1. The lower end of the cylindrical cell shown represents the sloping earth surface while the upper end is at a height of approximately 1000 m (i.e. above the surface boundary layer). The diagram to the right represents the vertical

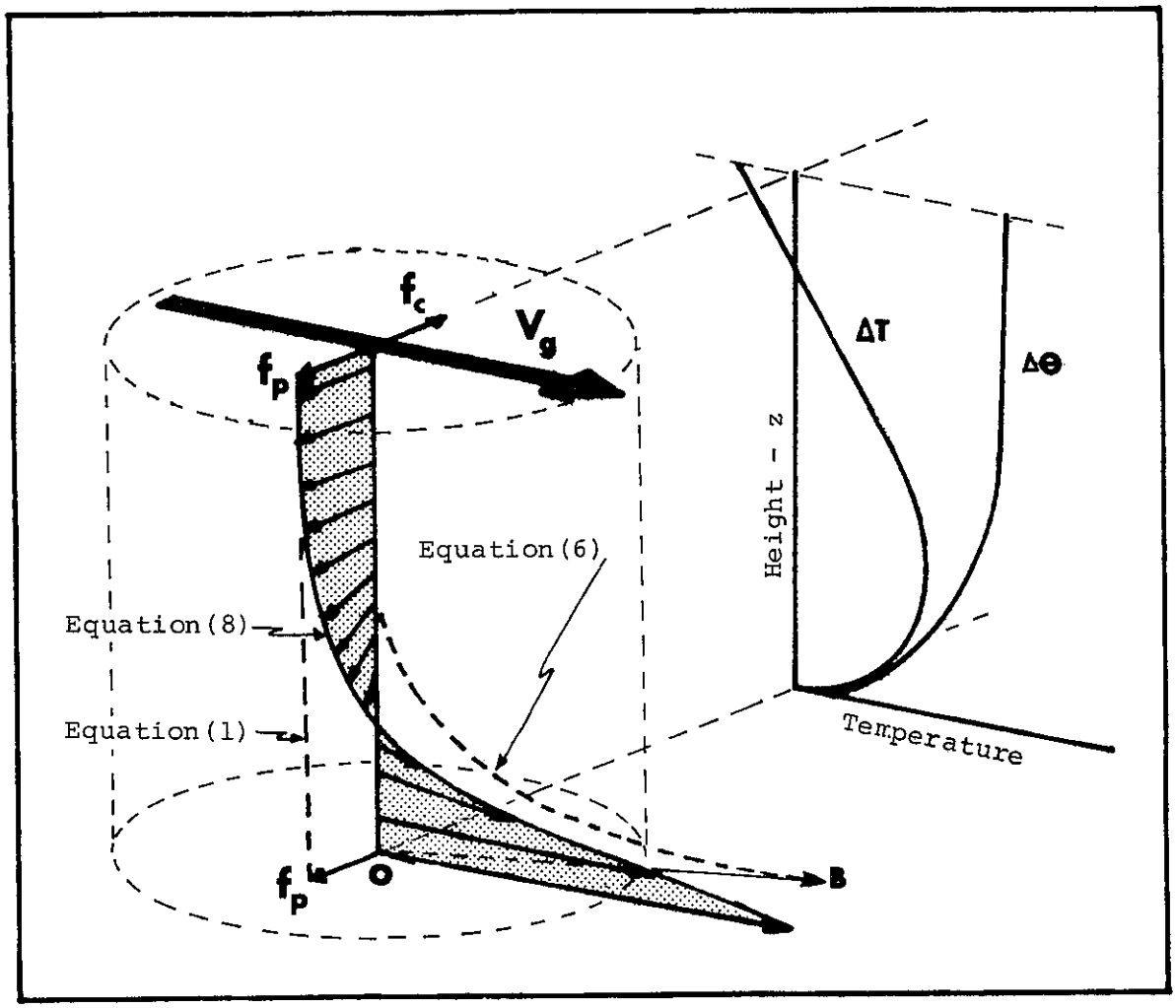

Figure 1. Diagram depicting the pressure gradient vector in the vertical structure model.

profiles of temperature (ΔT) and potential temperature ($\Delta\theta$). The terrain is sloping in the direction $\overrightarrow{OB}$. At a large distance from the ground and over laying the stable surface air layer, the geostrophic wind $\vec{V}_g$ is shown. If one assumes that the equations of geostrophic balance apply (Hess 1969), then the force due to the synoptic pressure gradient, f_p, and the Coriolis force, f_c, are equal and opposite and $\vec{V}_g$ is directed along the isobars. The synoptic pressure gradient is given for the x direction by

$$\frac{\partial p}{\partial x} = \rho\lambda v_g \quad \text{and} \quad \frac{\partial p}{\partial y} = \rho\lambda u_g \qquad .....(1)$$

where $\lambda = 2\Omega\sin\psi$.

The pressure gradient, $\vec{\nabla}p$, is transmitted through the atmospheric boundary to the surface as shown.

When stable air moves over a sloping terrain, it experiences a body force which is directed down the slope (i.e. along $\overrightarrow{OB}$). Consider the hydrostatic equation for air

$$\frac{\partial p}{\partial z} = -\frac{gp}{RT} \qquad .....(2)$$

Carrying out logarithmic differentiation with respect to x gives

$$\frac{\partial^2 \ln p}{\partial x \partial z} = \frac{g}{RT^2}\frac{\partial T}{\partial z} \qquad .....(3)$$

and taking x to be in the direction $\overrightarrow{OB}$

$$\frac{\partial T}{\partial x} = \left(\frac{\partial T}{\partial z} + \Gamma\right)\frac{\partial h}{\partial x}\,. \qquad .....(4)$$

Combining equations (3) and (4) and integrating with respect to z gives the pressure gradient at height z to be

$$\left(\frac{\partial p}{\partial x}\right)_z = \frac{gp}{R}\left(\frac{1}{T(H)} - \frac{1}{T(z)} - \Gamma\int_z^H \frac{dz}{T^2}\right)\frac{\partial h}{\partial x} \qquad .....(5)$$

Over the height of interest the variation of pressure with z may be neglected. Furthermore the integral in Equation (5) may be approximated

without undue error by $(H-z)/\bar{T}^2$. With these approximations, (5) simplifies to

$$\left(\frac{\partial p}{\partial x}\right)_z = \frac{-g}{\bar{\rho}\bar{T}} \left(\theta(z) - \theta(H)\right) \frac{\partial h}{\partial x} \qquad .....(6)$$

The values of $\left(\theta(z) - \theta(H)\right)$ are obtained from measured vertical temperature profiles. The form of equation (6) has been plotted on Figure 1 as well as the resultant pressure vector. It is seen that the down slope pressure force vanishes rapidly with height and the resultant pressure vector rotates clockwise, in the case illustrated, until only the synoptic pressure gradient remains at a height of the order of 500 m.

Since the velocity gradients in the x- and y- directions are small, one may neglect horizontal transfer of momentum so that the equation of motion (Sutton 1953 p 70), may be written for the x-direction as

$$\frac{du}{dt} = \frac{\partial}{\partial z}\left(K(z)\frac{\partial u}{\partial z}\right) + \lambda v - \frac{1}{\rho}\frac{\partial p}{\partial x} \qquad .....(7)$$

If one assumes that the motion is steady, then the acceleration term on the left of equation (7) is zero.

The first term on the right represents the rate of momentum diffusion followed by the Coriolis force and the pressure force. The pressure term is given by (1) and (6) as

$$\frac{\partial p}{\partial x} = \frac{-g}{\bar{\rho}\bar{T}} \left(\theta(z) - \theta(H)\right) \frac{\partial h}{\partial x} + \bar{\rho}\lambda v_g \qquad .....(8)$$

and

$$\frac{\partial p}{\partial y} = \bar{\rho}\lambda u_g \qquad .....(8a)$$

The form of the momentum diffusivity K(z) is for the present taken to be of the form (Sutton 1953 p 85)

$$K(z) = K_o Z^n \qquad .....(9)$$

The boundary conditions are

$$z = 0 \qquad u = 0 \qquad v = 0$$
$$z \to \infty \qquad u \to u_g \qquad v \to v_g \qquad \text{.....(10)}$$

The solution of Equation (7) has been given by Kohler (Sutton 1953 p 243) for a synoptic pressure gradient alone (Equation (1)) and this leads to a result which is similar to the Ekman spiral (Sutton 1953 p 70).

The integration of Equations (7), (8) and (9) with boundary conditions (10) has been carried out numerically. Temperature data required in Equation (8) were obtained directly from temperature profile measurements, (see Figures 2 and 3). The results of the numerical integration are shown in Figures 4 and 5 along with experimental data obtained in the Richards Bay area. For lack of any detailed information on the diffusivity, K(z), n in Equation (9) was taken to be 0,1; K_o was regarded as a free constant and was chosen to give reasonable agreement with theory. This procedure is adequate to demonstrate the model despite the obvious shortcomings of the assumed diffusivity profile.

What emerges from the data shown in Figures 4 and 5 which enables one to proceed further with wind field modelling is that near the surface both the Coriolis force and the rate of downwards momentum transfer from the overlying geostrophic wind may, to a good approximation, be neglected relative to the pressure forces given by Equation (8).

This is shown by the experimental data where the observed wind direction at 10 m is in close agreement with the direction of the resultant vectorial sum of the pressures given in Equation (8) (see arrow indicated in Figures 4 and 5). This is a most significant result for use in the surface wind field model. One could not draw this conclusion from the vertical structure model probably due to too high an assumed diffusivity near the surface. Clearly further work needs to be done on the vertical structure model and the purpose of presenting the analysis at this stage is to assist with the surface wind field modelling.

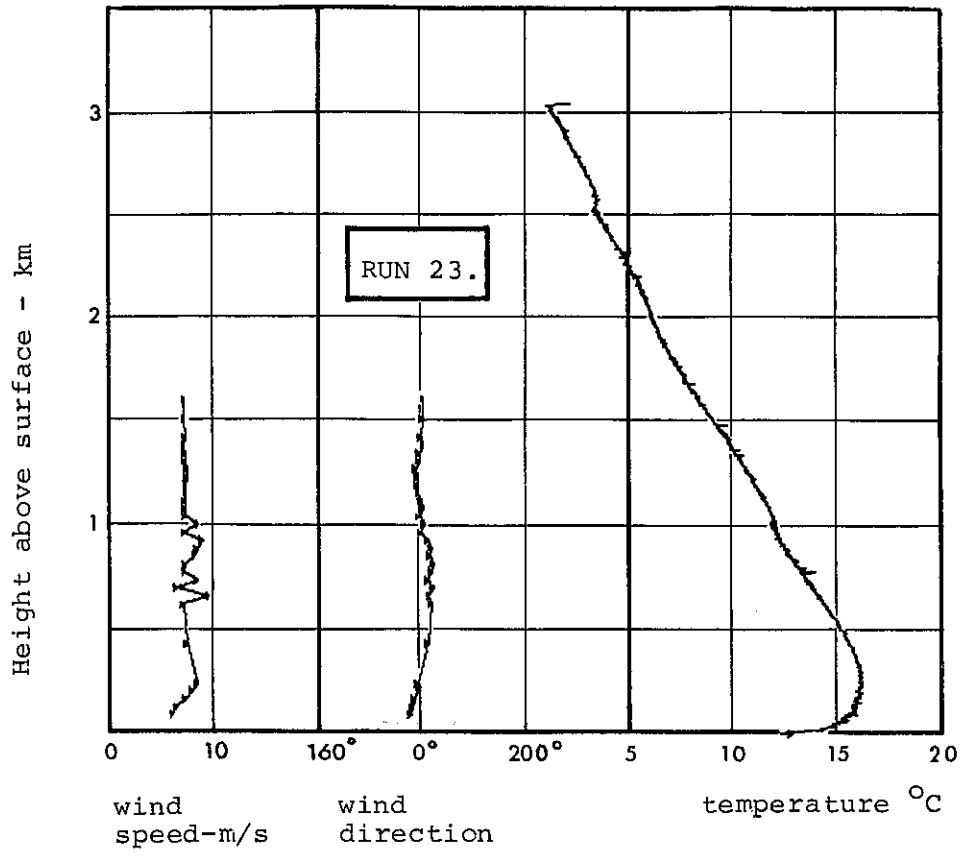

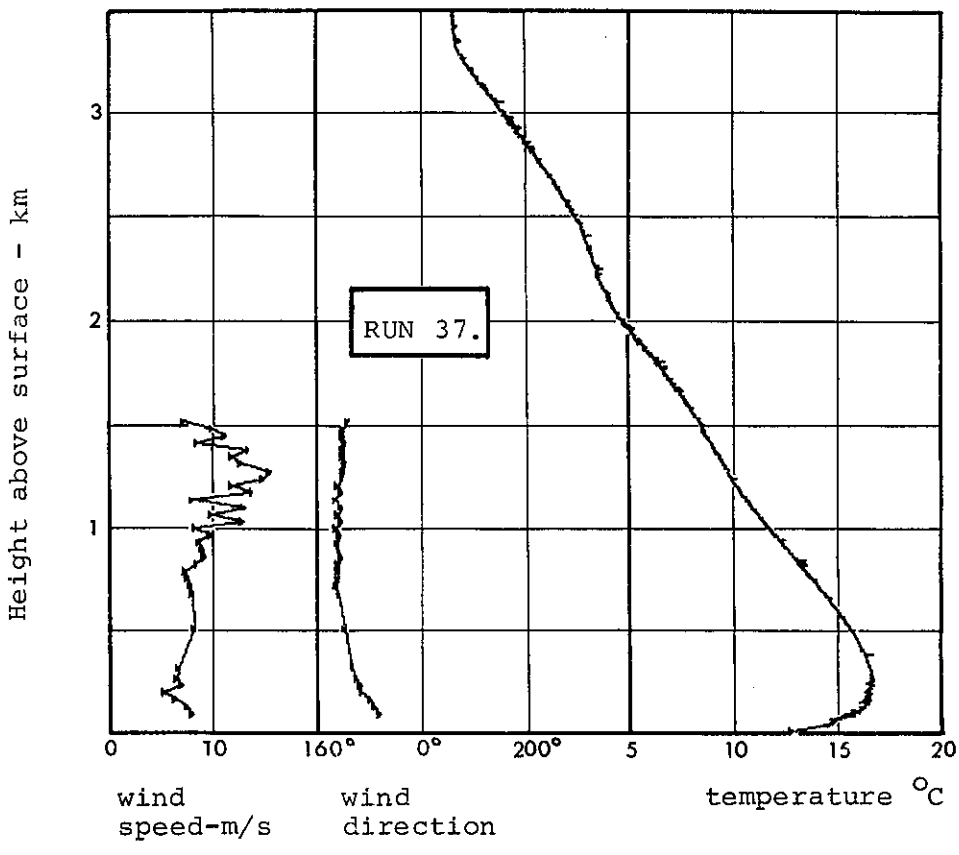

Figures 2(a) and 2(b). Measured vertical profiles of wind velocity and air temperature.

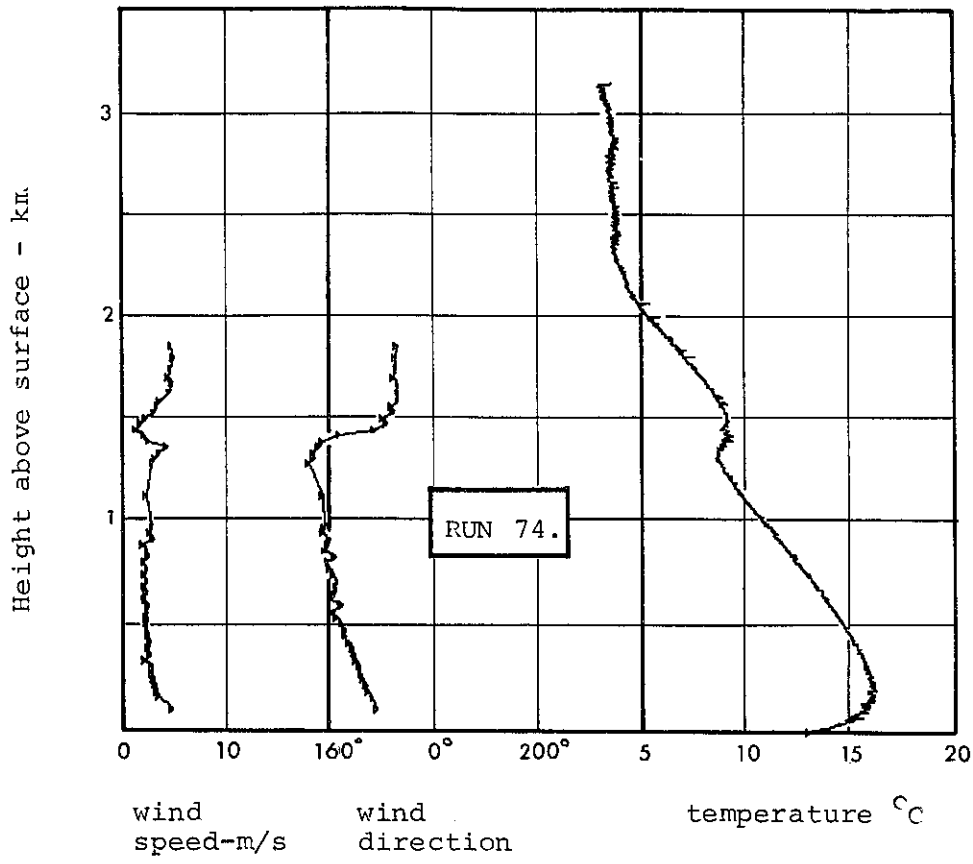

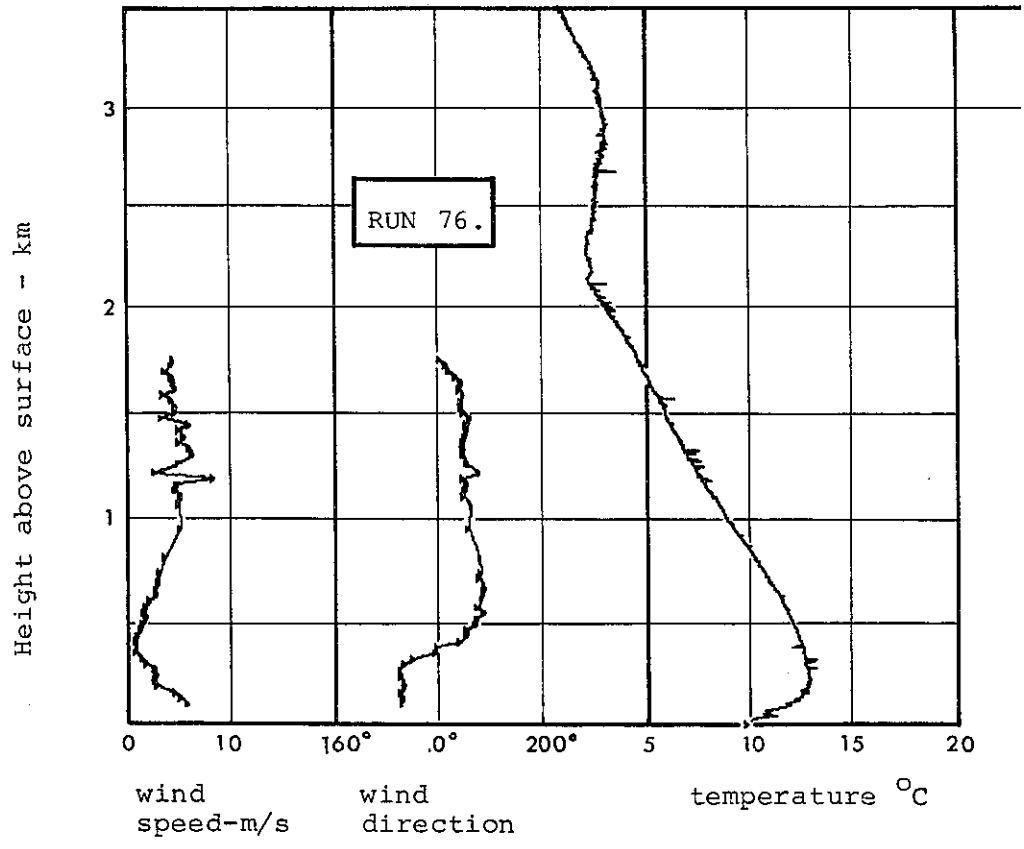

Figures 3(a) and 3(b). Measured vertical profiles of wind velocity and air temperature.

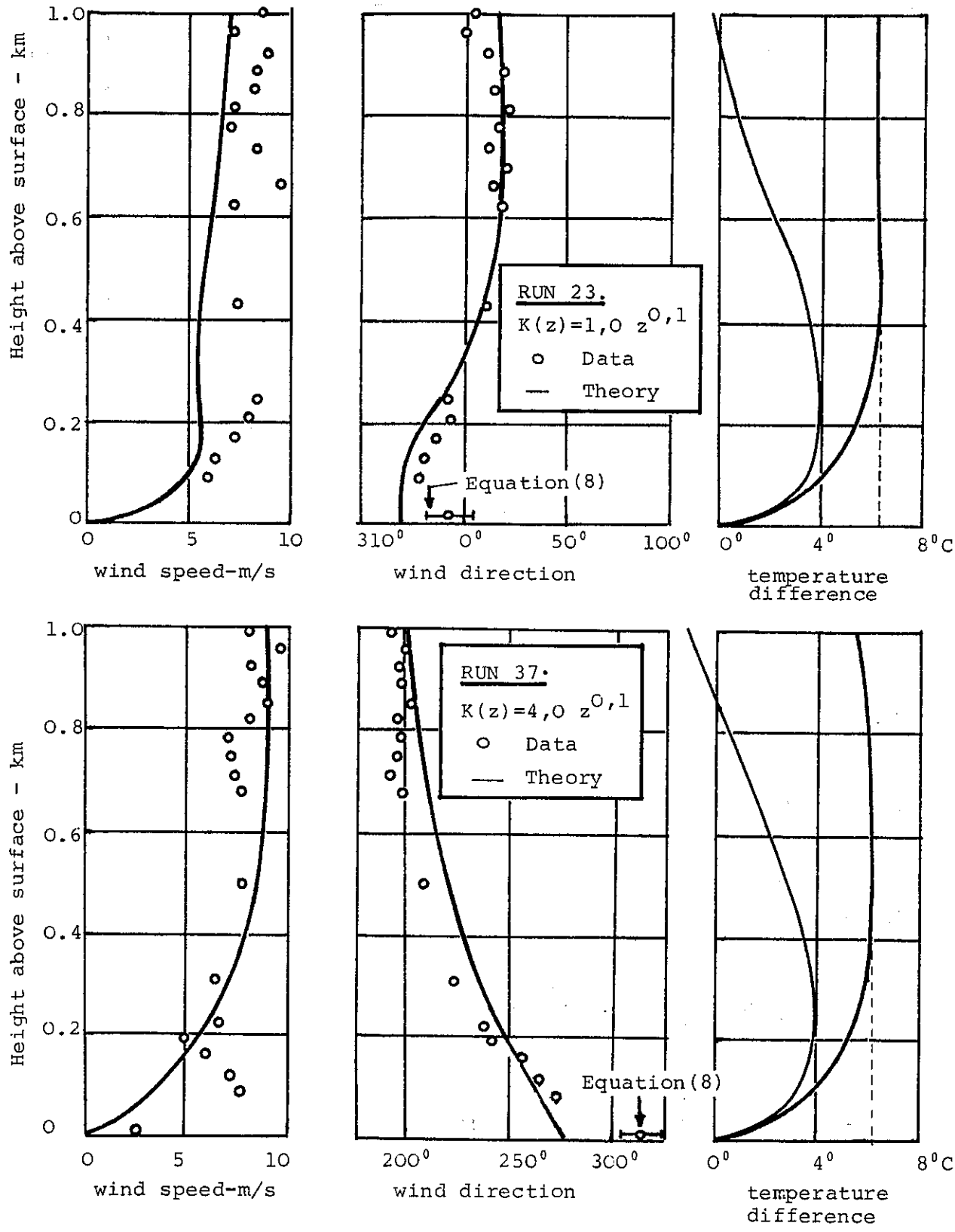

Figures 4(a) and 4(b). Comparison between experimental data and the vertical structure model.

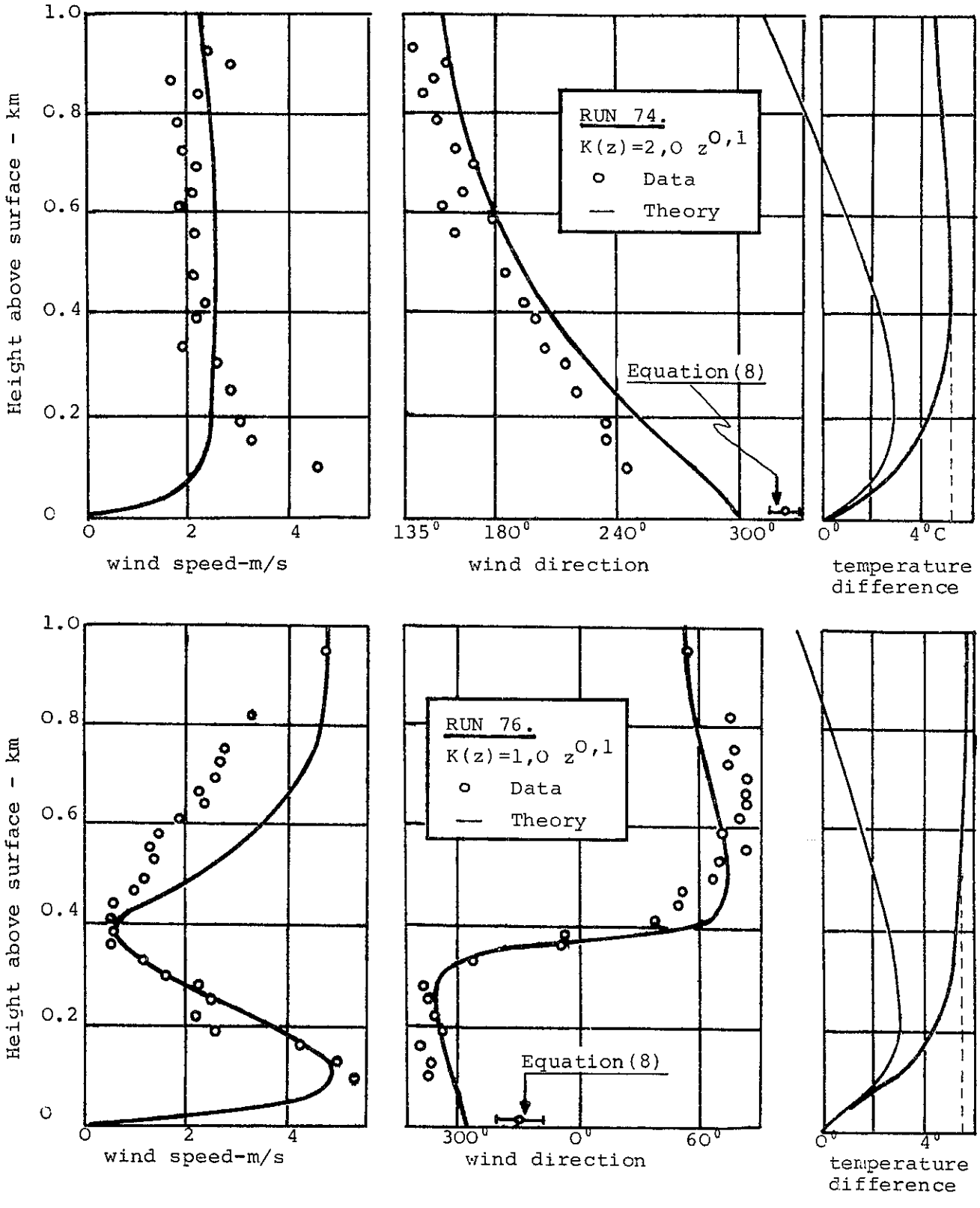

Figures 5(a) and 5(b). Comparison between experimental data and the vertical structure model.

It is therefore implied by the data that within the surface layer

$$\frac{1}{\rho}\frac{\partial p}{\partial x} = \frac{\partial}{\partial z}\left(K(z)\frac{\partial u}{\partial z}\right) \qquad .....(11)$$

where the pressure term is given by Equation (8).

Averaging Equation (11) over the surface layer by integrating from h to H' gives

$$\frac{1}{\rho}\frac{\overline{\partial p}}{\partial x} = K(z)\frac{\partial u}{\partial z}\Bigg|_{h}^{H'}\frac{1}{(H'-h)} \qquad .....(12)$$

where H' represents an arbitrary height above the surface below which the directional shear is not large.

Furthermore, for low speed stable flows which tend to laminar flow behaviour, and neglecting variations in surface layer thickness, Equation (12) may be further approximated by

$$\frac{1}{\rho}\frac{\overline{\partial p}}{\partial x} = -K(z)\left(k\,\bar{u}\right) \qquad .....(13)$$

If the surface friction is assumed uniform and the lateral transfer of momentum is neglected (a reasonable assumption since lateral velocity gradients are small) then

$$\bar{u} = k_f\frac{\overline{\partial p}}{\partial x} \qquad .....(14)$$

and a two dimensional flow potential function ϕ can be introduced such that

$$\bar{u} = \frac{\partial \phi}{\partial x} \qquad .....(15)$$

Hence one concludes from a study of the vertical structure, with the foregoing assumptions, that the stable flow within the surface air layer may be approximated by two dimensional potential flow theory with

$$\frac{\partial \phi}{\partial x} = k_f\frac{\partial p}{\partial x} \qquad .....(16)$$

The constant k_f is related to the drag coefficient.

The concepts expressed in Equations (8) and (16) are the basis of the wind field model.

Surface wind field model

From the results of the previous section, it is concluded that the motion of surface air (below H') is primarily determined by the distribution of surface pressure. Air movement is from regions of higher pressure towards those of lower pressure. The topography will modify the flow paths by obstructing and channelling the surface air.

At a land/sea interface, a further pressure gradient other than those given by Equation (8) must be included. This additional gradient of pressure is due to the difference in air temperature over the land and over the sea giving rise to the land breeze (Tyson and Preston-Whyte 1972). This pressure gradient is approximately normal to the coastline.

The problem of surface windfield prediction for a general complex topography now reduces to the *a priori* estimation of the pressure gradients given by Equation (8) as well as that due to a land breeze for a land/sea interface. By using the continuity equation (Schlichting 1968), channelling effects of topography are included in the model and it is therefore ensured that no spurious divergences or convergences appear in the flow field. This latter consideration is of the utmost importance for dispersion modelling in a complex region. The present method of predicting the topographical influence on wind fields is due originally to Anderson (1971), although some of Anderson's approximations have been abondoned since they were considered inappropriate for shallow stable flows.

The continuity equation for flow may be written

$$\frac{\partial u}{\partial x} + \frac{\partial v}{\partial y} = -\frac{\partial w}{\partial z} \qquad \text{.....(17)}$$

Averaging Equation (17) through the surface layer by integrating from h to H' gives

$$\overline{\frac{\partial u}{\partial x}} + \overline{\frac{\partial v}{\partial y}} = - \left[\frac{w(H') - w(h)}{H' - h}\right] \qquad .....(18)$$

It is assumed that the stable surface air is constrained to move between the topography, h, and H'. Both h and H' are functions of x and y. The surface H'(x,y) was modelled by smoothing the topography h(x,y) (shown in Figure 6) and displacing this smoothed surface upwards by 50 m. Smoothing was done by fitting two-dimensional cubic splines to the topography (Ahlberg *et al* 1967). The advantage of using cubic splines is that the cut-off point for short wavelengths is very sharp and is easily controlled. The minimum wavelength included by the filter for H' is approximately 11 km. The choice of H' = 50 m is somewhat arbitrary and represents the specification of a surface layer in which the assumptions leading to Equation (11) apply.

The vertical velocity, w(h), at the ground represents the upflow or downflow induced as the air layer moves over the surface, i.e.

$$w(h) = \vec{V} \cdot \vec{\nabla} h$$

and

$$w(H') = 0 \qquad .....(19)$$

Introducing the flow potential, (Equation (15)) Equation (18) becomes

$$\nabla^2 \phi_1 - \frac{\vec{\nabla}\phi_1 \cdot \vec{\nabla} h}{(H'-h)} = 0 \qquad .....(20)$$

The boundary conditions for Equation (20) are determined by the land breeze and synoptic pressure gradients.

The synoptic pressure gradient, assuming geostrophic balance, is given by Equation (1). Estoque (1961) has given a numerical solution of the equation of motion in two dimensions for the land/sea breeze circulation which shows for the land breeze that subsidence occurs over the land and air rises over the sea. The size of the circulation cell so set up

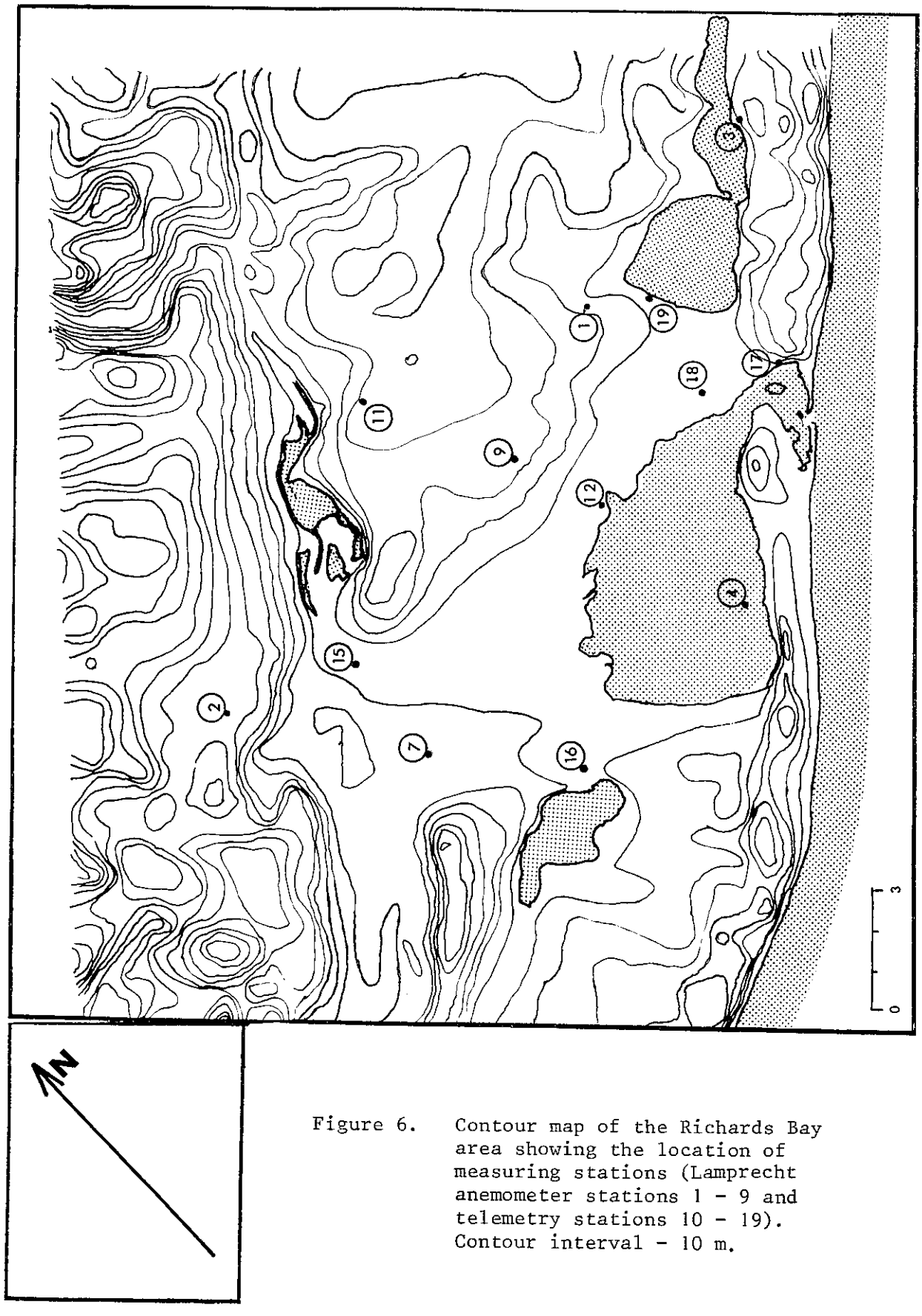

Figure 6. Contour map of the Richards Bay area showing the location of measuring stations (Lamprecht anemometer stations 1 - 9 and telemetry stations 10 - 19). Contour interval - 10 m.

extends from 98 km inland to 50 km over the sea. Anderson (1971) suggests that a fair degree of realism may be obtained for regions of non-uniform surface temperature if the subsidence velocity in Equation (18), w(H'), is represented by $A(T_o - \bar{T})$ where T_o is the local surface temperature and $\bar{T}$ is the area-average surface temperature in the region. This is the form of the land breeze solution adopted for this work. Equation (18) was solved on a coarse grid extending from 101 km inland to 48 km out to sea. Since the vertical extent of the land breeze is much greater than H', the height of the measured temperature inversion H_I, (approximately 250 m, see Figures 2 and 3) was used instead of H' in Equation (18) giving

$$\nabla^2\phi - \frac{\nabla\phi\cdot\nabla h}{(H_I-h)} = -\frac{A(T_o - \bar{T})}{(H_I - h)} \qquad .....(21)$$

The surface H_I in Equation (21) was a smoothed version of the topography with a cut-off wavelength of 58 km. The strength of this filter is not critical since the objective is only to eliminate unrealistic regional divergence or convergence from the boundary conditions supplied by this solution for the subsequent interior fine grid solution.

The downslope pressure field is incorporated in the model as follows: From Equations (6) and (18), the velocity gradient between the topography and surface H' due to the slope induced flow and due to perturbation of the flow by the topography is

$$\nabla^2\phi_3 - \frac{\vec{\nabla}\phi_3\cdot\vec{\nabla}h}{(H'-h)} = k_f\Delta\theta_s\nabla^2 h_f \qquad .....(22)$$

Other than very near the surface, the slope vector in Equation (22) (from Equation (8)) will not represent the topographical slopes in the finest detail but represents the general slope of the immediate region. It is therefore necessary to filter out the finer details of the topography such as short steep slopes giving the surface h_f. The filter used for computing the gradient ∇h in Equation (22) had a cut-off wavelength of approximately 3 km.

From Equation (22) one obtains

$$\nabla^2\phi_3 - \frac{\vec{\nabla}\phi_3 \cdot \vec{\nabla}h}{(H'-h)} = k_f \Delta\theta_s \nabla^2 h_f \qquad \ldots\ldots(23)$$

Approximate boundary conditions are obtained from Equation (23) by neglecting the topographical perturbation term which gives $\phi_3 = h_f$.

The procedures for computing the potential flow field are summarised in the diagram overleaf.

Since Equation (20) is linear, separate solutions for the geostrophic and land breeze potential gradients may be obtained and subsequently added to simulate any combination of the separate effects. For all solutions the constants and other parameters were set equal to unity as indicated in the diagram, so providing what have been termed 'unit solutions'. Since the equations are linear, these unit solutions may subsequently be added with the appropriate constants and parameters as multipliers to give the combined potential field. Numerical integrations were carried out using methods due to Peaceman and Rachford (1955).

A coarse grid solution for the synoptic potential gradient was carried out so that the boundary conditions used for the interior fine grid solution would at least reflect perturbations due to the large scale features of the topography. Separate unit solutions for gradients in each of the two coordinate directions were obtained, as shown in the diagram. These unit solutions may be added to synthesize any geostrophic pressure vector.

The final potential field is obtained by compounding the unit solutions, constants and parameters as follows:-

$$\phi = A(T_0 - T_s)\phi_1 + k_f\left(\bar{\rho}\lambda\left(u_g\phi_{2y} + v_g\phi_{2x}\right) + \frac{g\Delta\theta}{\bar{\rho}\,\bar{T}}s\phi_3\right) \qquad \ldots\ldots(24)$$

Velocities and air trajectories are obtained from the potential field using 'steepest descent' methods.

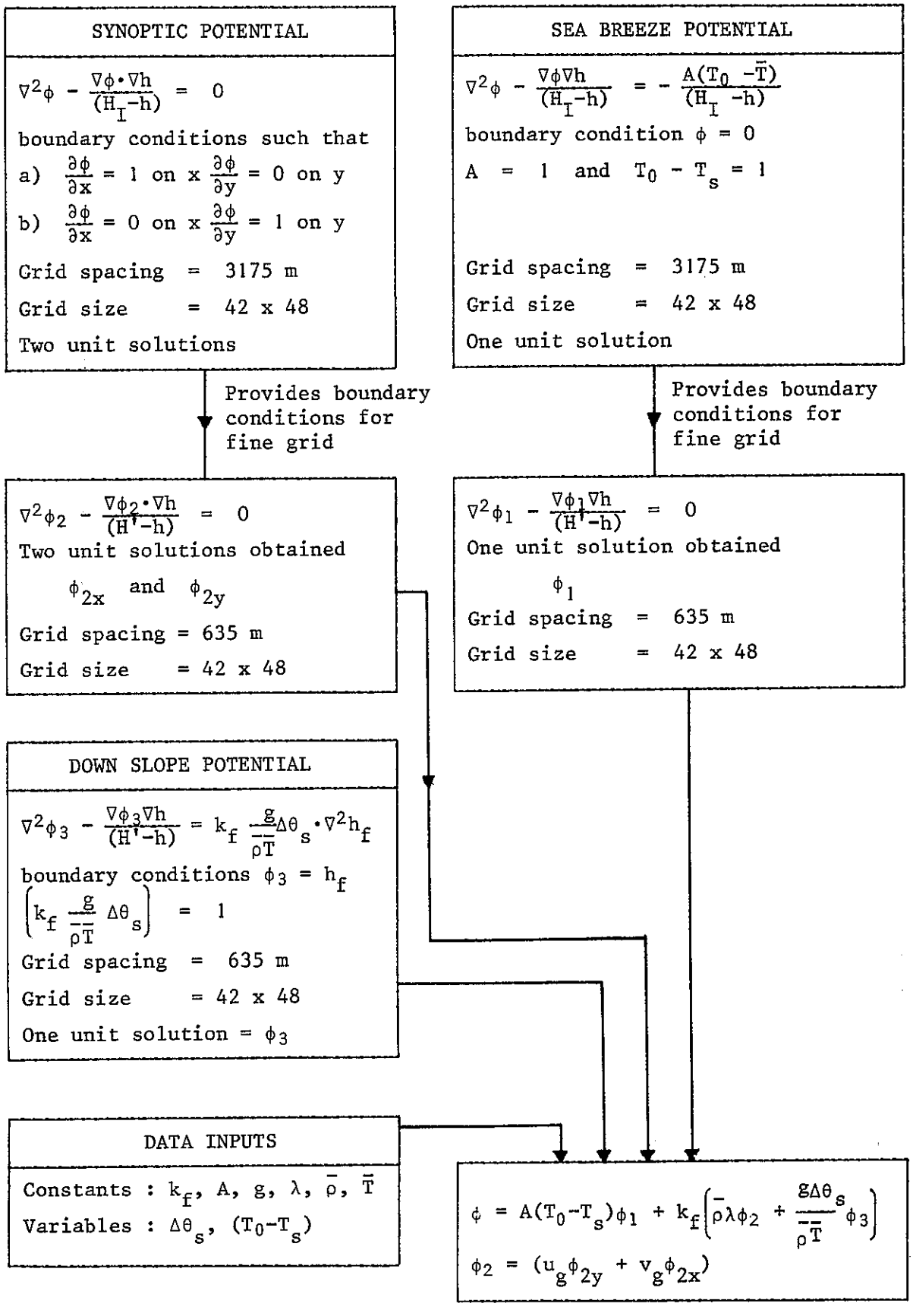
SYNOPTIC POTENTIAL
$\nabla^2\phi - \frac{\nabla\phi \cdot \nabla h}{(H_I - h)} = 0$
boundary conditions such that
a) $\frac{\partial\phi}{\partial x} = 1$ on x $\frac{\partial\phi}{\partial y} = 0$ on y
b) $\frac{\partial\phi}{\partial x} = 0$ on x $\frac{\partial\phi}{\partial y} = 1$ on y
Grid spacing = 3175 m
Grid size = 42 x 48
Two unit solutions
SEA BREEZE POTENTIAL
$\nabla^2\phi - \frac{\nabla\phi \nabla h}{(H_I - h)} = - \frac{A(T_0 - \bar{T})}{(H_I - h)}$
boundary condition $\phi = 0$
A = 1 and $T_0 - T_s = 1$
Grid spacing = 3175 m
Grid size = 42 x 48
One unit solution
Provides boundary conditions for fine grid
Provides boundary conditions for fine grid
$\nabla^2\phi_2 - \frac{\nabla\phi_2 \cdot \nabla h}{(H' - h)} = 0$
Two unit solutions obtained
ϕ_{2x} and ϕ_{2y}
Grid spacing = 635 m
Grid size = 42 x 48
$\nabla^2\phi_1 - \frac{\nabla\phi_1 \nabla h}{(H' - h)} = 0$
One unit solution obtained
ϕ_1
Grid spacing = 635 m
Grid size = 42 x 48
DOWN SLOPE POTENTIAL
$\nabla^2\phi_3 - \frac{\nabla\phi_3 \nabla h}{(H' - h)} = k_f \frac{g}{\bar{\rho}\bar{T}} \Delta\theta_s \cdot \nabla^2 h_f$
boundary conditions $\phi_3 = h_f$
$\left(k_f \frac{g}{\bar{\rho}\bar{T}} \Delta\theta_s\right) = 1$
Grid spacing = 635 m
Grid size = 42 x 48
One unit solution = ϕ_3
DATA INPUTS
Constants : k_f, A, g, λ, $\bar{\rho}$, $\bar{T}$
Variables : $\Delta\theta_s$, $(T_0 - T_s)$
$\phi = A(T_0 - T_s)\phi_1 + k_f\left(\bar{\rho}\lambda\phi_2 + \frac{g\Delta\theta_s}{\bar{\rho}\bar{T}}\phi_3\right)$
$\phi_2 = (u_g\phi_{2y} + v_g\phi_{2x})$

EXPERIMENTAL PROGRAM

In order to test the viability of the theoretical models for predicting both the wind fields and the vertical wind structure, it was necessary to carry out an extensive program of field measurement. This program involved the simultaneous mearsurement of wind speed and direction at a large number of sites in the area and the measurement of temperature and wind velocity profiles in the first 3000 m of the atmosphere. Dispersion measurements were also made, using an airborne tracer, for dispersion modelling work which is not presently discussed.

Wind field measurements

The wind velocity was measured using nine recording Lamprecht anemometers and a further eight Casella Sensitive anemometers together with wind direction vanes mounted on 10 m masts. The Lamprecht anemometers were permanently installed over a region along the coast extending from 35 km south west of Richards Bay to 25 km in the north east and 16 km inland (Station numbers in Figure 6 up to 9). Year-round records were obtained from these instruments. The sensitive anemometers were mounted on semi-portable masts and were deployed in the immediate vicinity of Richards Bay (Station numbers in Figure 6 between 11 and 19). These instruments were only used during the winter period. The semi-portable masts also carried instruments for measuring wind speed and temperature at 1 m level as well as at the 10 m level. The data from all these instruments were encoded and telemetered every 3 minutes via a UHF radio link to a central receiving station located at Station 9 (see Figure 6). At the central station the data were decoded, displayed and recorded on magnetic tape, for subsequent computer processing. This telemetry system for on-line wind field information greatly facilitated the experimental work.

Vertical wind and temperature structure

The vertical structure of the lower 3000 m was obtained by theodolite tracking and ascending 100 g meteorological balloon. The balloon release point was at Station 9 in Figure 6. The balloon carried a temperature transmitter (temperature sonde) specifically developed for this work. Air

temperature was sensed by an aspirated, fast response thermistor bead, 0,25 mm in diameter. The thermistor was used to modulate an oscillator which in turn pulse modulated an f.m. transmitter. The instrument required no calibration other than the noting of a reference oscillator frequency and temperature at the ground before release. The rate of ascent was approximately 2,2 m/s and the temperature signal received at the ground gave the temperature at 1 second intervals. Based on laboratory measurement, the instrument precision is estimated to be 0,035°C per degree temperature change from the surface air temperature, which is used as a reference temperature. Figures 2 and 3 give typical temperature profiles measured by the temperature sonde. These data were recorded on magnetic tape for decoding into computer permanent file.

RESULTS AND DISCUSSION

It is emphasised that all the data reported in this paper are for the winter period of June - mid-August 1975 and all conclusions and generalisations therefore apply only to the winter months.

The theoretical work reported presupposed that the geostrophic balance equation, Equation (1), may be used to obtain the geostrophic pressure gradient from the measured vertical profiles of wind speed and direction. Below the 2 km level the vertical profiles of temperature shown in Figures 2 and 3, with the possible exception of that for Run 74, are simple in the sense that above the surface based inversion the lapse rate is approximately uniform and is in good agreement with the US Standard Atmosphere Lapse Rate (SALR) of -6,5°C/km (Hess 1969). The curve marked $\Delta\theta_s$ in Figures 4 and 5 is a plot of potential temperature based on the SALR rather than the Dry Adiabatic Lapse Rate (DALR) of -9,8°C/km. From these data it would appear that, while the temperature inversion depth (from the ΔT curve) is of the order of 200 to 300 m, the thermal boundary layer, which is of greater thermal stability than the standard atmosphere, extends up to 300 or 400 m for the runs shown. These inversion depths are fairly typical of all runs between 22h00 and sunrise. A large proportion of the vertical profile data do not show the simple vertical structure implied by the temperature profiles of Runs 23, 37 and 76. The lapse rates above the

surface layers are in some cases very different from either the DALR or the SALR and in many cases further strong inversion layers appear in the first 2 km. It is unlikely that Equation (1) or Equation (6) would apply in these complex cases. At this stage of the analysis of the Richards Bay data, only those runs exhibiting a simple temperature profile have been examined in order to gain some understanding of the surface wind fields. The four runs currently reported (with the possible exception of Run 74) all show simple temperature profiles and were selected to demonstrate the effect of various geostrophic wind strengths and directions. The vertical structure model and the surface wind field model are compared with the data for these four runs. The analysis of the runs showing complex temperature profiles is in progress but the work has not progressed sufficiently for inclusion at this stage.

Vertical profiles of wind speed and direction

Equation (8) for computing the vertical profile of downslope pressure gradient would indicate then if the DALR, (Γ), is used in this equation, then the standard atmosphere, even in the absence of a more stable surface layer, would experience a downslope body force. It is assumed that the standard atmosphere is stable on an incline and the DALR in Equation (8) has been replaced by the SALR for use in the vertical structure model.

The solid lines in Figures 4 and 5 (other than in the temperature plots) represent the results of the numerical integration of the vertical structure model. As discussed in the section on the vertical structure model (pp 2-7), the form of K(z) was taken to be

$$K(z) = K_o z^{0.1} \qquad .....(25)$$

K_o was regarded as a free parameter and was chosen for each run so as to achieve reasonable agreement with the experimental data. The values of K_o used are given in the graphs.

From the results of other workers the experimental form of the diffusivity profile used here is not adequate. Indications are that the diffusivity reaches a maximum at some distance above the ground and then falls to a small residual value at heights of the order of 1 km (O'Brian 1970).

Inferior correlation between theory and experiment was found when the local slope vector, $\frac{\partial h}{\partial x}$, in Equation (6) was used. Over a 1 km distance downwind from the point of balloon release the slope was estimated from a topographical map to be 0,021 towards 155^{o}. A lesser slope of 0,014 towards 144^{o} gave better correlation and was used for all the model results shown.

Further work needs to be done on the vertical structure model and the purpose of presenting these results at this stage is to provide a basis for the modelling of the surface wind fields. From a comparison between experiment and theory in Figures 4 and 5, it would appear that the prediction of wind direction profiles (other than near the surface) is reasonably good, while the predicted wind speed profiles show only good qualitative agreement with the data. Figure 5(b) for Run 76 shows fairly complex wind speed and direction profiles. At the time of this run, assuming geostrophic balance, the geostrophic pressure gradient and the downslope pressure force from Equation (6) were almost directly opposed. The agreement between the model prediction and experimental data shown in Figure 5(b) is considered satisfactory. Data for Runs 37, 74 and 76 show that below approximately 200 m the wind speed increases to a maximum before decreasing to zero at the ground. Under similar conditions, similar maxima were measured near the surface in the Cape Town area. Other than for Run 76, this maximum is not shown by the model. The form of the momentum diffusivity profile chosen, Equation (25), is unlikely to be realistic (as has been discussed) and this could explain the relatively poor agreement with the wind speed data.

In the modelling of the vertical structure the land breeze pressure gradient which is approximately normal to the coast line and which would also vanish above the thermal boundary layer, has not been explicitly included. At the location at which the vertical profile data were taken, the land breeze pressure gradient would be approximately in the direction of the down-slope pressure gradient given by Equation (6). From a study of the wind fields it is inferred that this land breeze pressure gradient is the same order of magnitude as the geostrophic pressure gradient, which is much weaker than the dominant downslope pressure force in the surface layer.

Unfortunately, with theodolite tracking of the ascending temperature sonde, no wind velocity data were obtained below 50 m. The model would indicate that in the first 50 m the change in wind direction is not large.

Wind fields

From the vertical profiles of wind speed the following geostrophic wind information is obtained:-

Table 1. Geostrophic wind information

Run Number	Date 1975	Time	Geostrophic Wind Speed	Direction
23	1 July	03h35	7,5 m/s	0^{o}
37	9 July	21h45	8,0 m/s	198^{o}
74	20 July	00h15	2,3 m/s	144^{o}
76	3 August	03h20	4,8 m/s	52^{o}

From records of sea temperature for 1970 and 1971 (Pearce 1972) the average sea temperature for the winter period was approximately $22^{o}C$. The surface air temperature from Figures 2 and 3 for the above runs was between $10^{o}C$ and $12,5^{o}C$. The value of $(T_0 - T_s)$ in Equation (24) was taken as $10,5^{o}C$ for all runs. Other values of variables in Equation (24) used for all four runs are:-

Mean air density	$\bar{\rho} = 1,23\ kg.m^{-3}$
mean air temperature	$\bar{T} = 285^{o}K$
acceleration due to gravity	$g = 9,8\ m.s.^{-2}$
Coriolis constant for latitude $28,75^{o}$	$\lambda = 7,01 \times 10^{-5}\ s^{-1}$
Inversion strength	$\Delta\theta_s = 8,7^{o}C$

Clearly the inversion strength, $\Delta\theta_s$ in Equation (24) would depend on the location and in the lower regions of the topography $\Delta\theta_s$ would be larger than that at the station 9 (See Figure 6). The following table gives the

surface air temperatures, T_0, at Stations 9 and 7. The topographic heights of these stations are also given.

Table 2. Surface air temperatures, T_0, at Stations 9 and 7

Run	Station 9 Elevation 40m		Station 7 Elevation 12m	
	T^oC	$\Delta\theta_s$	T^oC	$\Delta\theta_s$
23	12,8	6,2	9,2	12,9
37	12,8	6,2	8,5	14,2
74	13,0	5,2	10,7	11,4
76	9,8	5,4	7,0	10,6

Assuming that the air temperature over the region is uniform at heights of the order of 400 m, the value of $\Delta\theta_s$ for Station 7 has been calculated using the elevation and temperature difference from Station 9 and the SALR. It is seen from Table 2 that the values of $\Delta\theta_s$ at Station 7 are approximately double those at Station 9, indicating much stronger temperature inversions at lower levels. The data of Langenberg (1967) taken in the valley below Station 9 at an elevation similar to Station 7 show inversions strength which are far greater than those presently reported at Station 9, this is consistent with the $\Delta\theta_s$ values reported in Table 2. A value of $\Delta\theta_s$ of $8,7^oC$ which is between those for Stations 9 and 7, has been used in Equation (24). In using this average value, the predicted downslope pressure gradient from Equation (6) is over-estimated by approximately 20% at higher elevations and under-estimated by approximately 30% at lower elevations.

The remaining two constants in Equation (24) which are required are A from Equation (21) and the constant k_f which relates pressure gradient and velocity (Equation 16). Rough *a priori* estimates of both these constants are possible but for the present it is preferred to estimate these two parameters from the experimental data. No regression scheme has yet been

attempted and the fitting of Equation (24) to the data using A and k_f was done by visual comparison of the predicted wind fields and that inferred from surface wind measurements giving A = 3,1 x 10^{-3} and k_f = -496.

The wind field predictions using Equation (24) and these values of A and k_f together with values of $\bar{\rho}$, $\bar{T}$, g, λ and $\Delta\theta_s$ as discussed are shown in Figures (7), (9), (11) and (13) corresponding with the geostrophic wind conditions given in Table 1.

In these figures are shown the surface pressure (or flow potential) distribution (dotted contours), and the associated air trajectories. The trajectory lengths are a measure of relative wind strength. Figures (8), (10), (12), (14) and (15) show the corresponding wind measurements for Runs 23, 37, 74 and 76. The relevant geostrophic wind and pressure gradient directions are shown in each of these figures calculated from Table 1 assuming geostrophic balance (Equation (1)). The approximate geostrophic pressure vector directions are onshore for Run 23, offshore for Runs 37 and 76 and mainly alongshore directed northwards for Run 74.

In the figures showing the experimental data, an interpolative technique due to Wendell (1972) has been used to aid in visualising the wind field implied by the simultaneous point wind measurements. Wendell's technique for N measuring stations is that for any grid point

$$u = \frac{\sum_{k=1}^{N} u_k/r_k^2}{\sum^{1}/r_k^2}$$

$$v = \frac{\sum_{k=1}^{N} v_k/r_k^2}{\sum^{1}/r_k^2} \qquad \text{.....(26)}$$

where r_k is the distance from station k.

Clearly the interpolated wind vectors have little significance in those areas of the figures which are remote from the data points shown. It is noted that the shorelines of the low lying swampy lakes shown on the

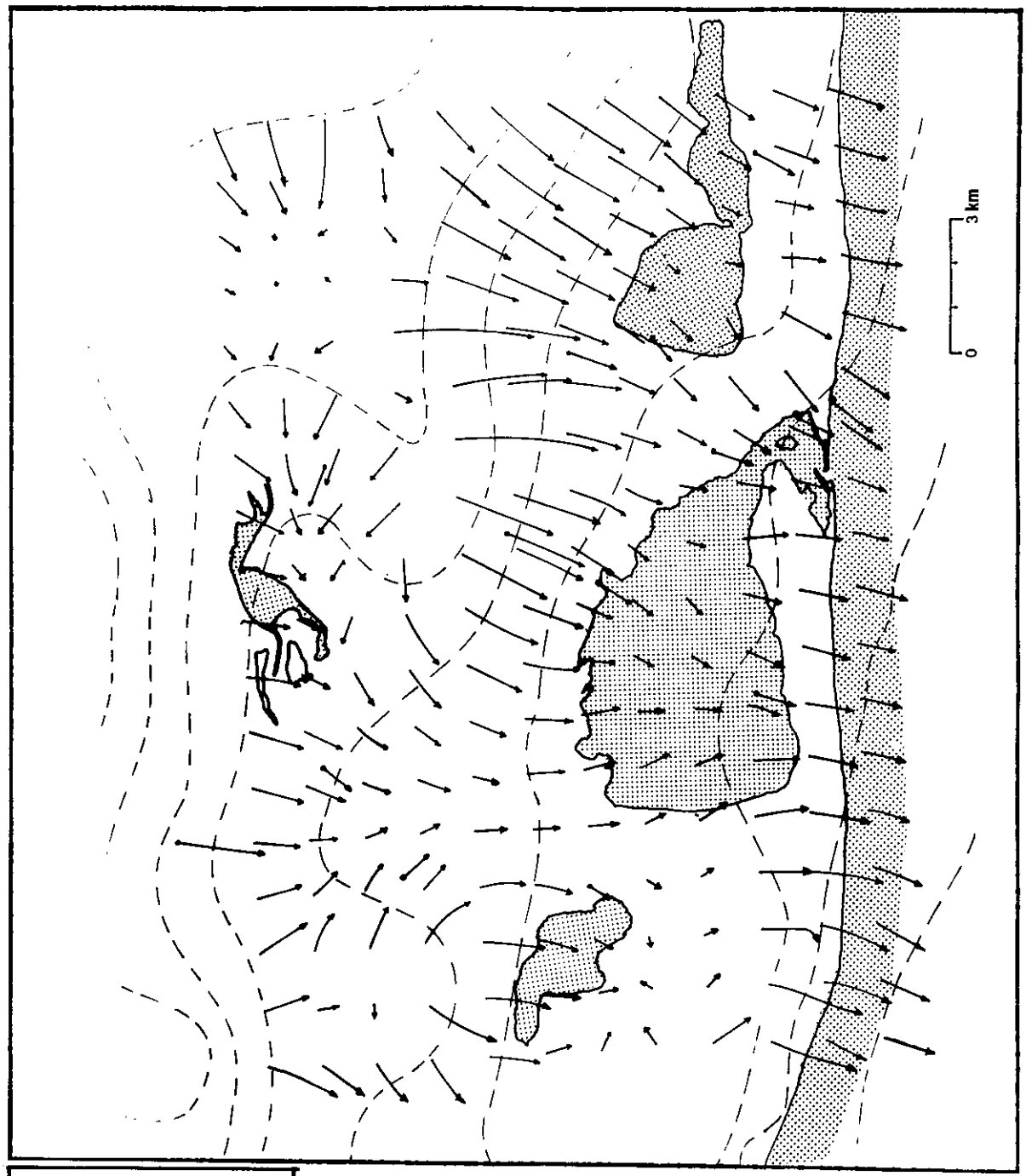

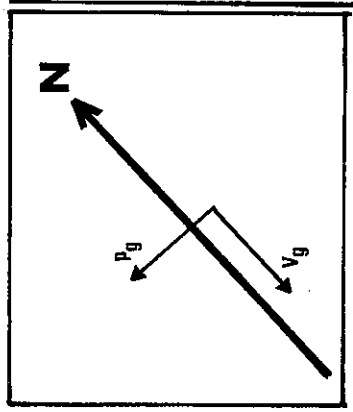

Figure 7. Model prediction of surface air trajectories for the conditions of Run 23. The dotted contours give the distribution of flow potential (pressure).

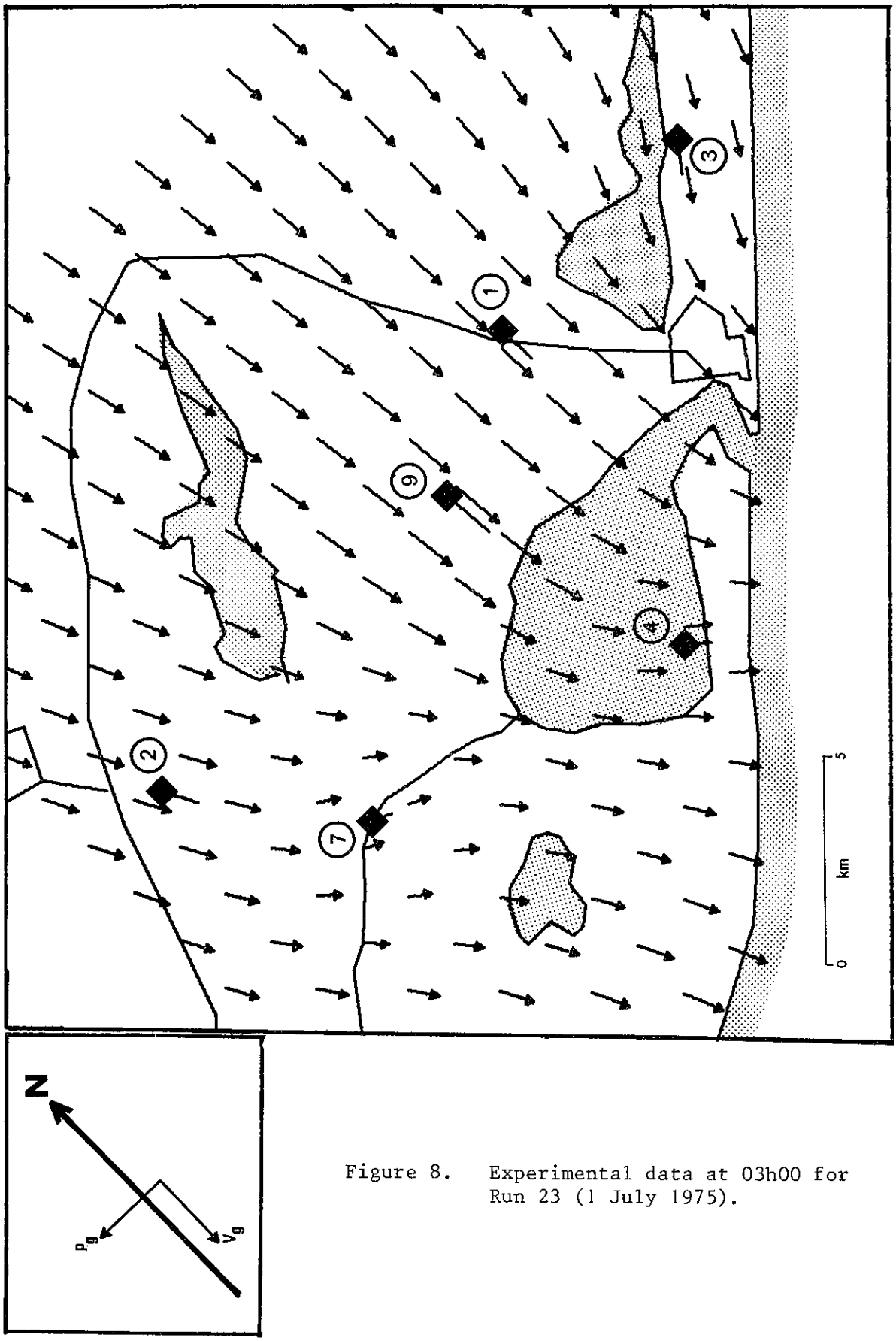

Figure 8. Experimental data at 03h00 for Run 23 (1 July 1975).

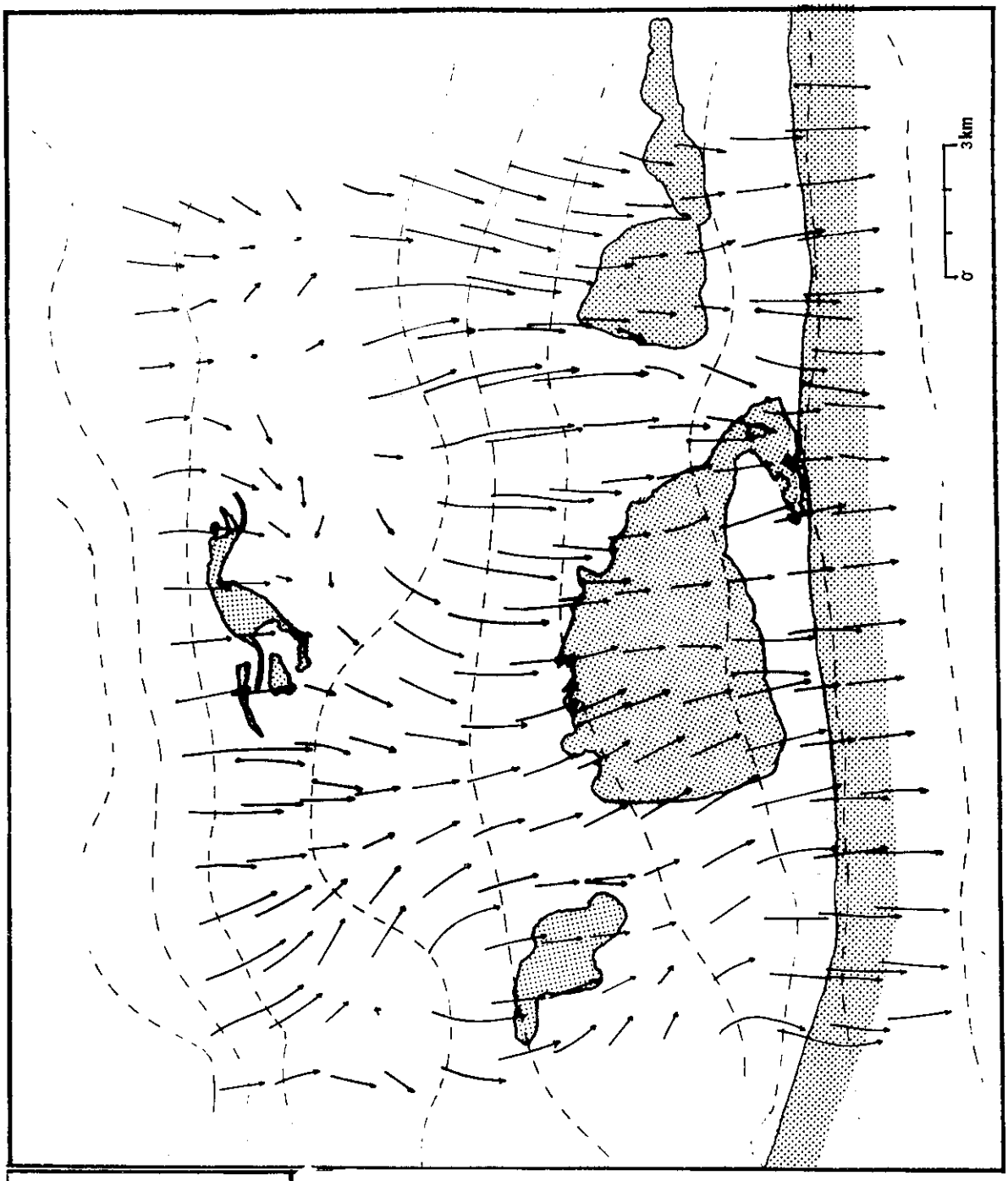

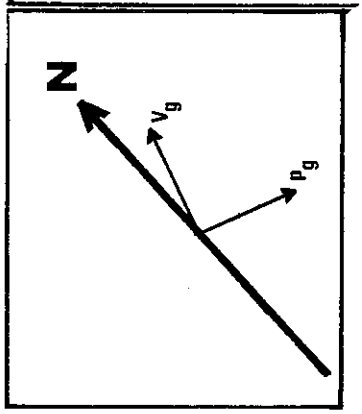

Figure 9. Model prediction of surface air trajectories for the conditions of Run 37. The dotted contours give the distribution of flow potential (pressure).

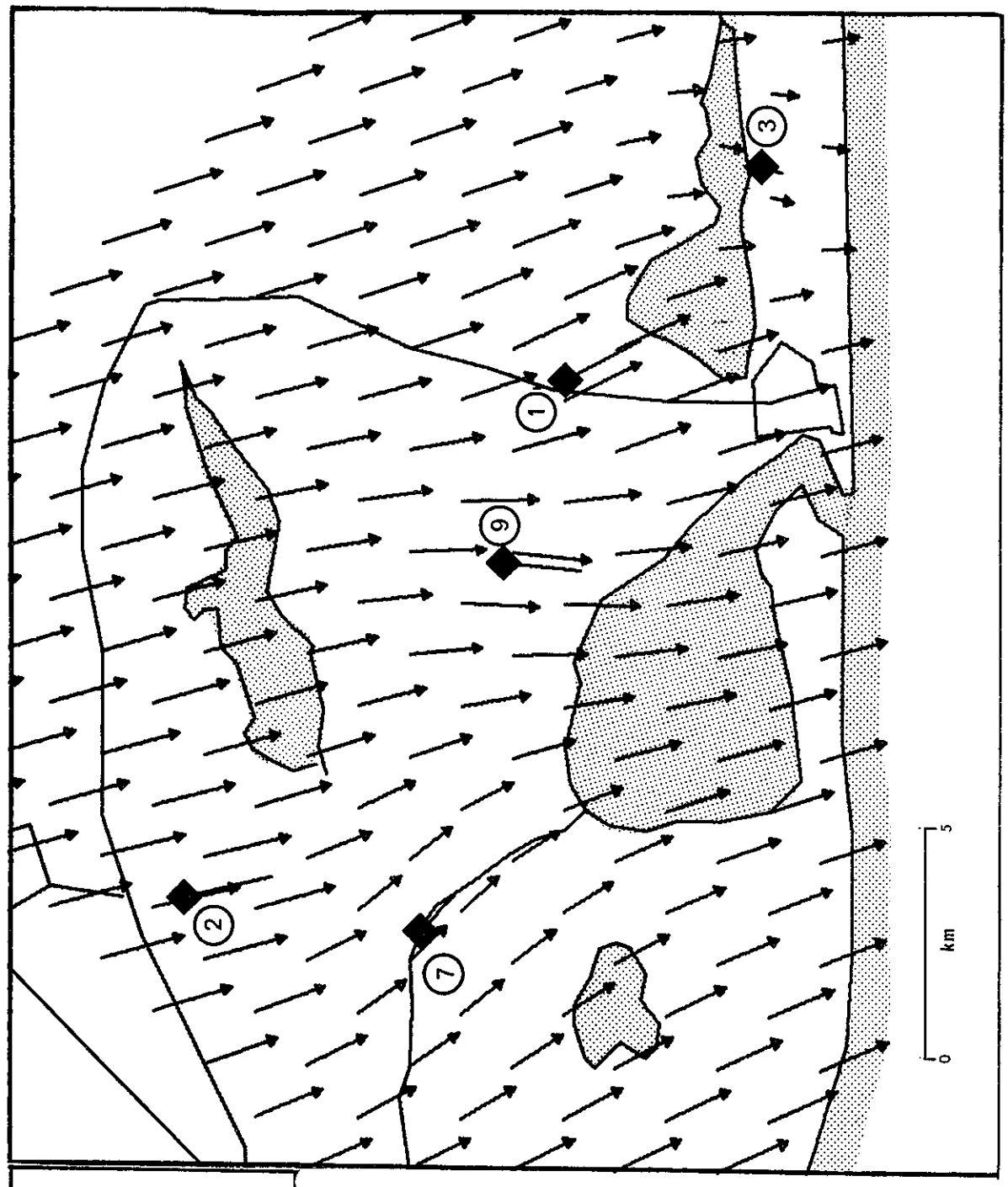

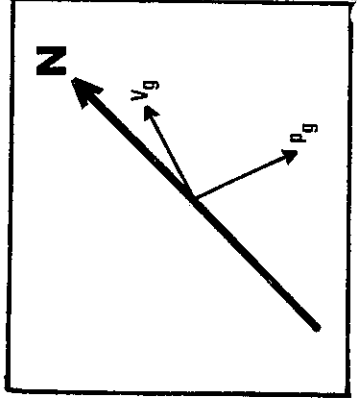

Figure 10. Experimental data at 22h00 for Run 37 (9 July 1975).

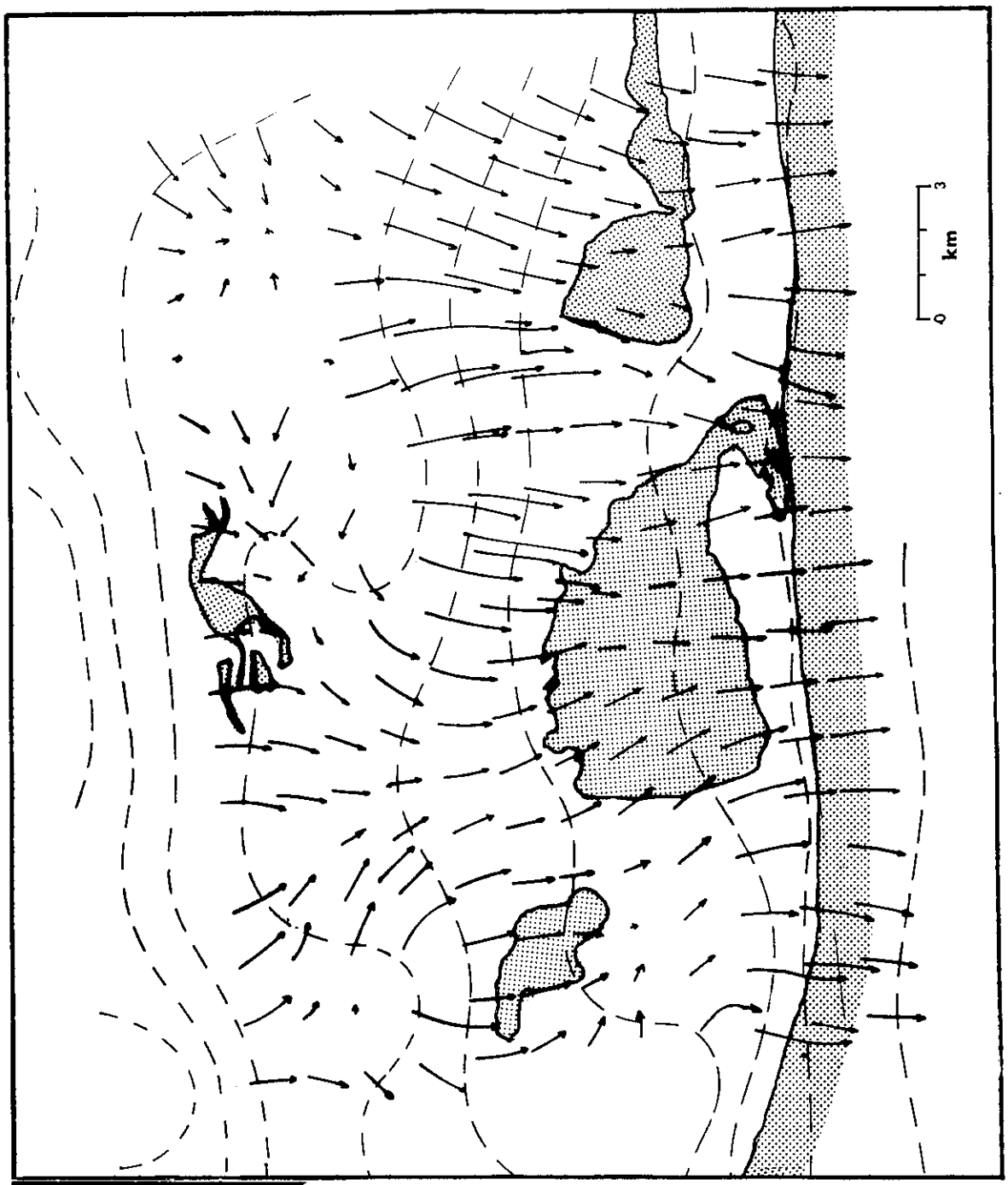

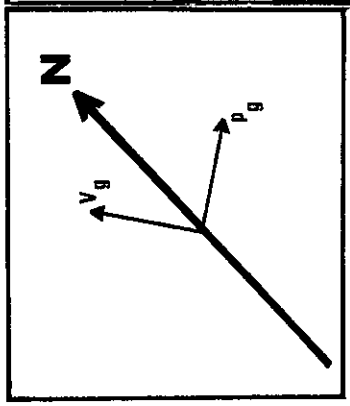

Figure 11. Model prediction of surface air trajectories for the conditions of Run 74. The dotted contours give the distribution of flow potential (pressure).

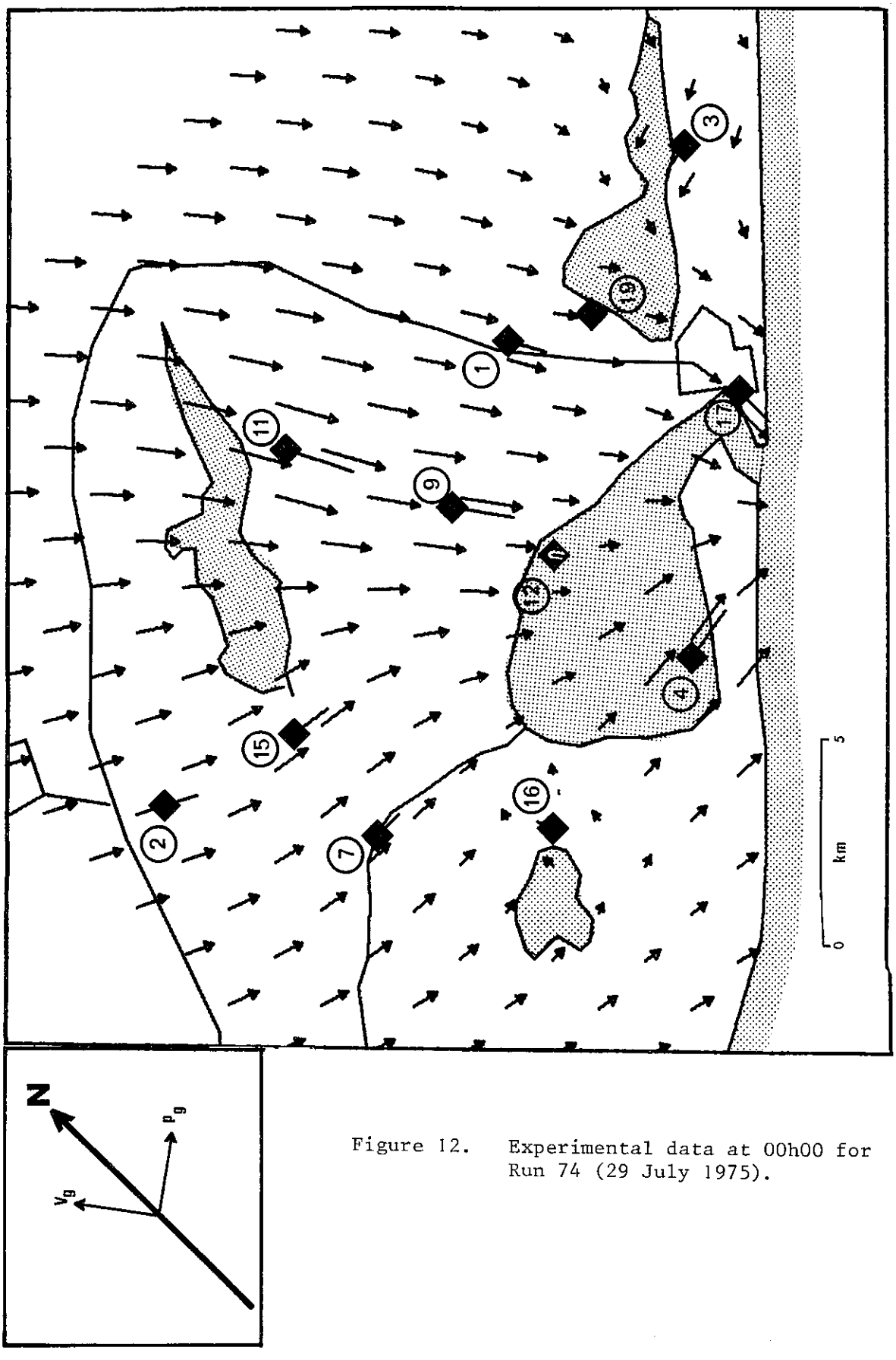

Figure 12. Experimental data at 00h00 for Run 74 (29 July 1975).

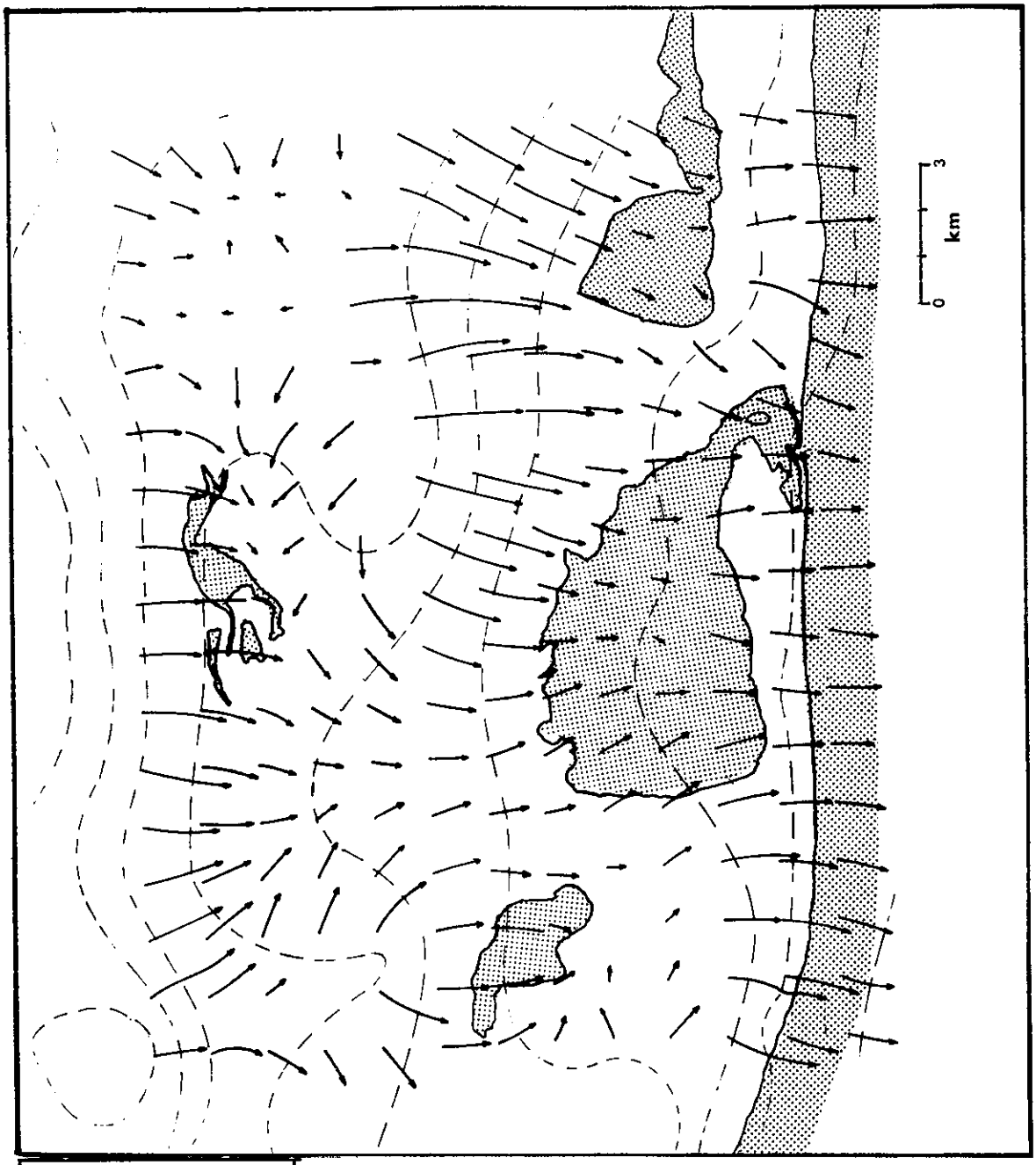

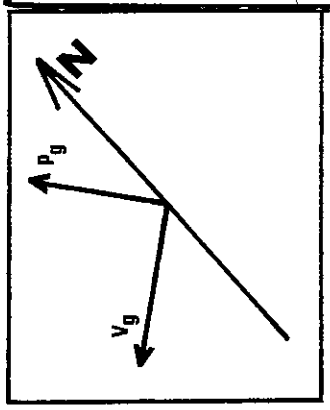

Figure 13. Model prediction of surface air trajectories for the conditions of Run 76. The dotted contours give the distribution of flow potential (pressure).

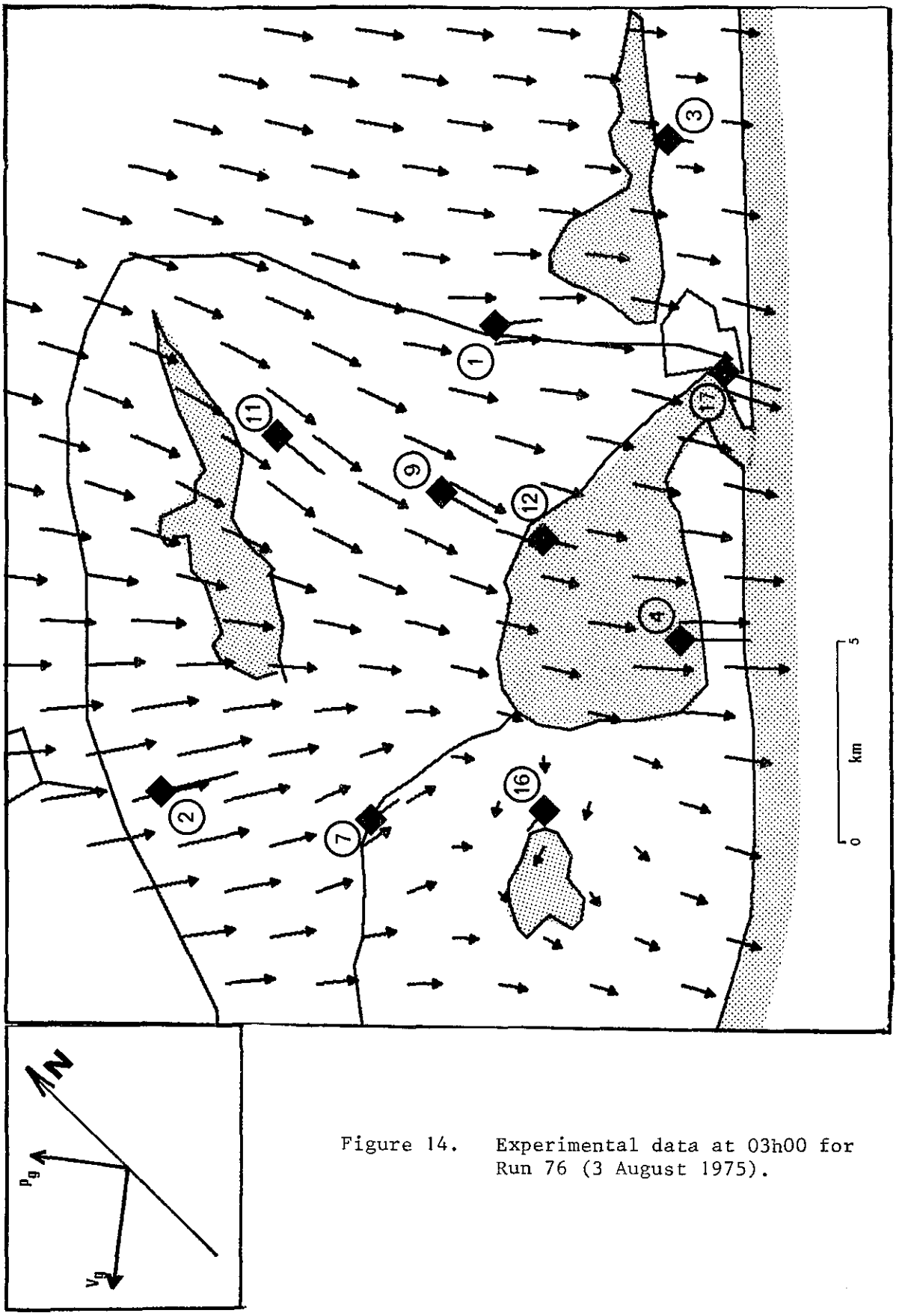

Figure 14. Experimental data at 03h00 for Run 76 (3 August 1975).

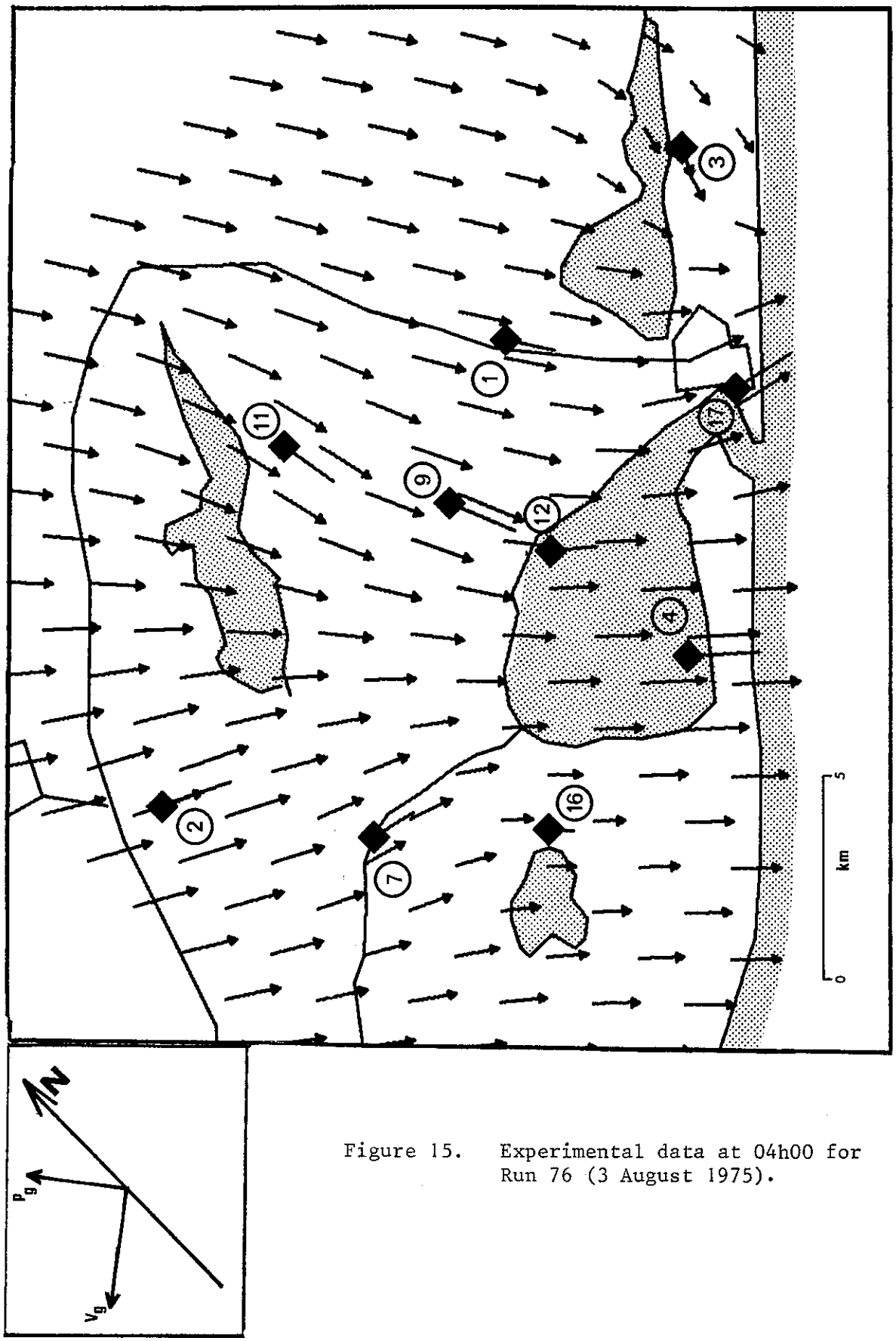

Figure 15. Experimental data at 04h00 for Run 76 (3 August 1975).

figures are somewhat different on the maps showing experimental data and those showing model predictions. The coordinates for the former maps were taken from a 1:250000 topographical map while the latter are from a 1:50000 scale map. These shorelines are likely to change with rainfall.

Comparing the predicted air trajectories with the experimentally inferred wind fields it is seen that in general the agreement is good. The convergence in the air movement down the valley near Station 7 and 15 (see Figure 6) which is predicted in all cases by the model is reasonably well shown by the experimental data within the resolution of the measurements using Wendell's interpolation method. There is also reasonable correlation between model and experiment in the general area of Stations 1, 9 and 12. The effect of the various geostrophic pressure gradient directions is well shown by the model which is in reasonable agreement with the experimental measurements except for Run 74. For this run, the data seem to indicate a somewhat stronger geostrophic gradient from the south west than is inferred from Figure 3(a) using Equation (1). Referring to this figure, it is seen that there is an inversion with its base at approximately 1,3 km and this run should probably be classed with those having a complex vertical structure, as discussed on pages 19 and 20.

In the general vicinity of Station 16, the model predicts for Run 23, 74 and 76 (Figures 7, 11 and 13) an area where the wind speeds are low and the wind directions are therefore indefinite. The measurements at Station 16 in Figures 12, 14 and 15 would imply the existence of a region of low pressure gradient such as that which is predicted by the model. Comparing the wind field data for Run 76 at 03h00 and 04h00 (Figures 14 and 15), it is seen that the wind vectors remained fairly constant over the one hour period with the exception of those at Stations 16, 3 and 17. Referring to the model predictions, it is seen that in the vicinity of Station 3 another region of low velocity is generally predicted which again appears to be in reasonable agreement with the data. The low pressure gradient areas would be associated with the pooling of stable air with the resultant accumulation of emitted pollutants from sources in these areas.

The model prediction at Station 11 is not good (See Figures 12, 14 and 15). The model indicates that air moves from Station 11 down into the valley on

the landward side. This predicted valley flow was not detected at Station 11. There are clearly other discrepancies between the model and experimental data, such as at Station 4 where predicted wind speeds are generally too low although the predicted wind directions are reasonably good.

In order to gain some idea of the resolution of the wind fields inferred from the data using Wendell's technique, simulated data from the model predictions of Run 76 (Figure 13) were used to generate Figure 16. It is seen that even with nine stations, much of the finer detail of the simulated wind field is lost.

Clearly there is a need for some regressional scheme to estimate the constants A and k_f once all the data have been analysed. The value of A and k_f obtained which gave reasonable correlation for the four runs shown are:-

$$A = 3,1 \times 10^{-3}$$
$$k_f = -496$$

A rough independent estimate of the value of A may be obtained from Estoque's solution by estimating the average subsidence velocity and average temperatures from Figure 14 of his paper (Estoque 1961). The centre of the convecture cell is approximately 600 m above the surface and it is at this level that the subsidence velocity was estimated giving $A = 3,03 \times 10^{-2}$. The subsidence velocity in the land breeze will decrease with height to zero at the surface and the relevant group for comparative purposes is A/H which for the above estimate gives

$$A/H = 2,27 \times 10^{-5} \qquad H = 600 \text{ m}$$

and for the present work

$$A/H = 1,24 \times 10^{-5} \qquad H = 250 \text{ m}$$

From unpublished data taken in 1972 at Cape Town by the authors, a value of

$$A/H = 1,95 \times 10^{-5} \qquad H = 213 \text{ m}$$

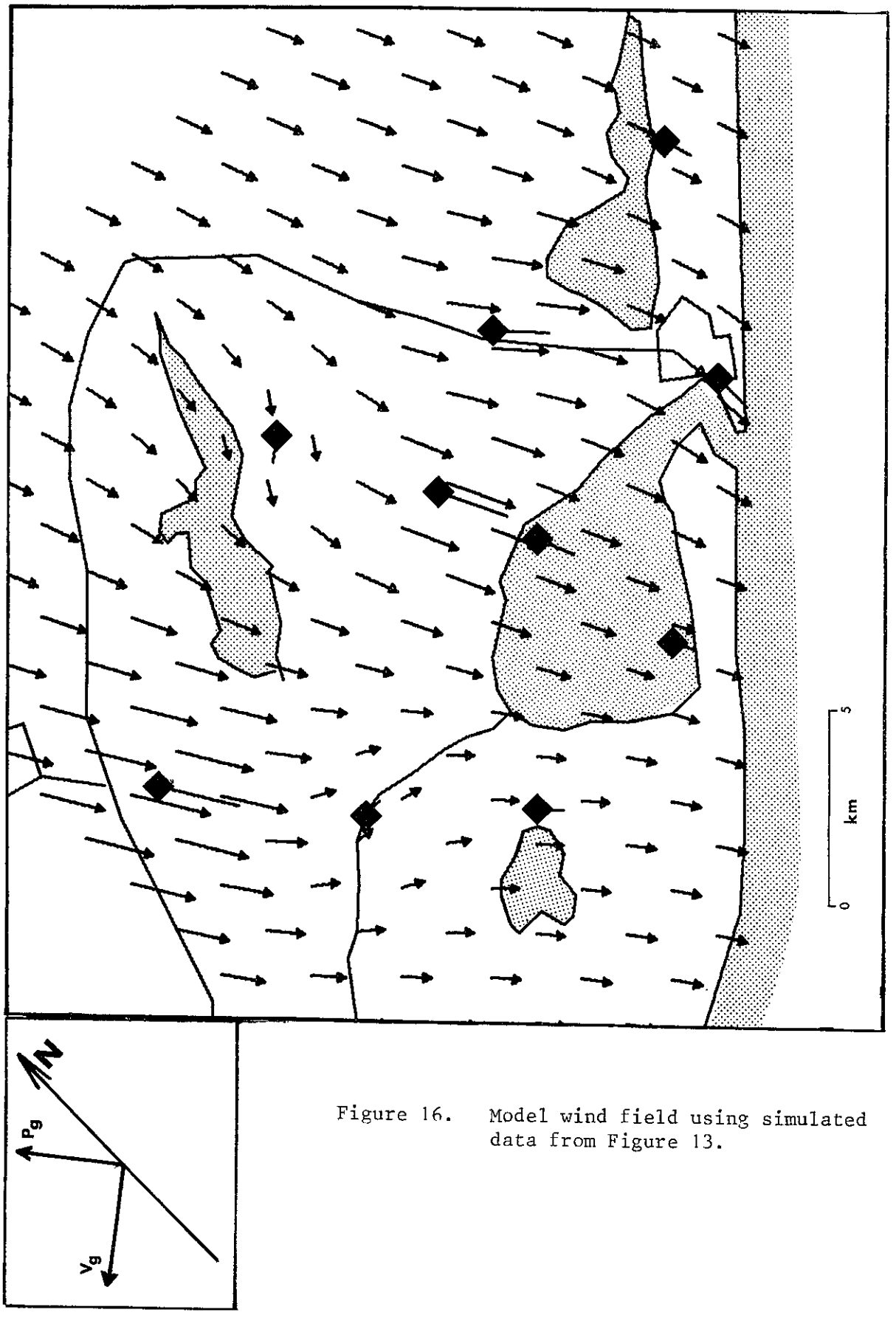

Figure 16. Model wind field using simulated data from Figure 13.

was obtained. The Cape Town value was obtained from wind data taken at 3 m and the model prediction did not include a downslope pressure gradient. By omitting the downslope pressure gradient from the model all of the pressure force is attributed to the $A(T_o-\bar{T})$ term which would increase the value of A/H estimated from the Cape Town data. This might explain the difference in the two experimental values of A/H reported.

An estimate of k_f can be made from Equation (11) by averaging over the surface layer from h to H' giving

$$\left(\frac{H'-h}{\bar{\rho}}\right)\frac{\overline{\partial p}}{\partial x} = \tau_{zx}(H') - \tau_{zx}(h) \qquad .....(27)$$

For stable flows which tend to laminar behaviour it is assumed that the shear stress at the ground is much larger than that at H'. Using Equation (14) gives

$$k_f = \frac{-\bar{u}(H'-h)}{\tau_{zx}(h)\bar{\rho}} \qquad .....(28)$$

An order of magnitude estimate of the surface shear stress under stable conditions may be obtained from Sutton (1953 p 243) as 1,5 dynes cm^{-2}. Taking $\bar{u} = 2$, $H' - h = 50$, and $\bar{\rho} = 1{,}23$ gives a value of $k_f = -542$. The relatively close agreement of this estimate with the value of -496 found from the data may be fortuitous in view of the assumptions regarding the values of the variables used in Equation (28). This calculation does however give the physical significance of k_f.

SUMMARY AND CONCLUSIONS

The flow of stable surface air over a region of complex topography has been studied. In order to understand the flow of surface air, it was necessary to measure and analyse the vertical profiles of wind velocity and temperature. A theoretical model for the vertical wind structure, up to 1 km, for stable air moving on an inclined surface with an overlying geostrophic wind is proposed. Using the hydrostatic equation for the variation of air

pressure with height, an expression for the down slope pressure profile in terms of the temperature inversion profile and the surface slope is derived (Equation (6)). This expression together with the geostrophic balance equation, is incorporated into the equation of motion. A simple exponential form was assumed for the vertical profile of diffusivity and the equations were numerically integrated.

Geostrophic wind information and temperature profiles for the integrations were obtained from the measurements. The model predictions were visually fitted to the wind velocity data using a single free parameter (K_0 in Equation (25)). Four runs representative of different geostrophic wind directions and strength were randomly chosen for analysis. The agreement between the model predictions and experiment is considered reasonably good (See Figures 4 and 5). Further work with the vertical structure model needs to be done giving special attention to the diffusivity profile. It is concluded from this study of vertical structure that for the range of geostrophic wind speed analysed (Table 1) the rate of momentum transfer from the geostrophic wind to the surface air layer is small and that the dominant force acting on the stable surface layer is due to the down slope pressure gradient (Figure 1).

Based on these findings from the vertical structure model, a surface air movement model is proposed.

For the surface wind field model, it is postulated that the movement of stable air near the surface is determined by the distribution of surface pressure. By assuming quasi-laminar flow behaviour and uniform surface friction, it is shown that the surface pressure distribution may be interpreted as a two dimensional flow potential field. The problem of wind field prediction is thus reduced to the prediction of surface pressure distribution, which is made up of the following components:-

(i) the overlying synoptic pressure gradient,
(ii) the land breeze pressure gradient, and
(iii) the downslope pressure gradient experienced by stable air moving on a slope.

By using the continuity equation, the blocking and channelling of the surface air by the topography are included in the model. The virtue of using a model based on the continuity equation is that spurious divergences

and convergences in the surface wind field are avoided. The final model equations are summarised by the diagram on page 17 which also gives the numerical procedures involved in the model predictions.

The wind field model includes two constants, A and k_f, as shown in the diagram on page 17. *A priori* estimates of both these constants is possible but for the present both constants were estimated from the experimental data. The values of A and k_f so obtained were in order-of-magnitude agreement with the *a priori* estimates.

The model results are shown in Figures 7, 9, 11 and 13 for the same periods used for the vertical structure analysis. The predicted wind fields shown in these figures are compared with experimental wind fields inferred from simultaneous wind measurements taken at a height of 10 m, at as many as twelve stations in the Richards Bay area. The agreement between the model predictions and experimental data is reasonably good. Some of the finer detail of the wind fields seems to be resolved by the model, which shows several regions where the wind speed is very low and the wind direction is therefore likely to be indefinite. The experimental data appear to verify the existence of these regions.

The results and conclusions in this paper are based on the analysis carried out to date on only part of the large volume of data taken in the Richards Bay area. It is emphasised that this work constitutes a theoretical basis for the analysis of data and the wind fields reported do not necessarily summarize the prevailing stable flows over the region.

REFERENCES

Ahlberg J H, Nilson E N, and Walsh J L 1967. *The Theory of Splines and Their Application.* Academic Press, New York.

Anderson G E 1971. Mesoscale Influences on Wind Fields. *J appl Meteorol* 10, 377-386.

Estoque M A 1961. A theoretical investigation of the sea breeze. *Q Jl R met Soc* 87, 136-146.

Hess S L 1969. *Introduction to Theoretical Meteorology.* Holt, Rinehart and Winston, New York.

Langenberg H M 1967. The climate, and the ventilation potential of the atmosphere, in the vicinity of Richards Bay. Part II. CSIR Report APRG/67/9.

O'Brian J J 1970. A note on the vertical structure of the eddy exchange coefficient in the planetary boundary layer. *J atmos Sci* 27(8), 1213-1215.

Peaceman P W, and Rachford H H 1955. The numerical solution of parabolic and elliptic differential equations. *J Soc ind & appl math* 3(1), 28-41.

Pearce D F 1972. Condensed tables of results of oceanographic research cruises by the *R V Meiring Naudé* of Richards Bay, May 1970 to March 1972. NPRL (Oceanographic Division) CSIR. Unpublished manuscript.

Schlichting H 1968. *Boundary Layer Theory.* 6th ed McGraw Hill, New York.

Sutton O C 1953. *Micrometeorology.* McGraw Hill, New York.

Tyson P D and Preston-Whyte R A 1972. *J appl Meteorol* 11(4), 643-650.

Wendell L L 1972. Mesoscale wind field and transport estimates determined from a network of wind towers. *Mon Weath Rev (USA)* 100(7), 565-578.

NOMENCLATURE

A	-	convection constant	m. s^{-1} $^{o}C^{-1}$
g	-	gravitational accelaration	m. s^{-2}
H'	-	height of top of surface layer above datum	m.
H_I	-	height of top of inversion layer above datum	m.
h	-	height of topographic surface above datum	m.
k_f	-	friction constant	m^4. $N.^{-1}$ s^{-1}
K(z)	-	vertical momentum diffusivity	m^2. s^{-1}
p	-	pressure	Pa
R	-	universal gas constant	J. $^{o}K^{-1}$ kg $mole^{-1}$
T	-	temperature	^{o}K
t	-	time	s
u	-	x-components of velocity	m.s^{-1}
v	-	y-components of velocity	m.s^{-1}
w	-	z-component of velocity	m.s^{-1}
V	-	horizontal velocity	m.s^{-1}
x,y	-	horizontal Cartesian coordinates	m.
z	-	vertical Cartesian coordinates	m.

Greek letters

ϕ	-	two dimensional flow potential	$m^2 s^{-1}$
Γ	-	dry adiabatic lapse rate	^{o}K m^{-1}
λ	-	Coriolis constant	s^{-1}
Ω	-	rotational speed of earth	s^{-1}
ψ	-	latitude	
θ	-	potential temperature	^{o}K
ρ	-	density	kg m^{-3}
$\Delta\theta_s$	-	potential temperature difference based on US Standard Atmosphere lapse rate	^{o}K

Subscripts

o - ground level

s - water surface, except $\Delta\theta_s$ (as above)

g - pertaining to the geostrophic wind

Over bar indicates an average

$\rightarrow$ indicates a vector